ARTICLES
https://doi.org/10.1038/s42255-020-0199-4
nature metabolism

Check for updates

Glucose-dependent partitioning of arginine to the urea cycle protects β-cells from inflammation

Accalia Fu[1,2], Juan Carlos Alvarez-Perez[3], Daina Avizonis[4], Tatsuya Kin[5], Scott B. Ficarro[1,6,7,8], Dong Wook Choi[1,2], Esra Karakose[3], Mehmet G. Badur[9], Lindsay Evans[1], Carolina Rosselot[3], Gaelle Bridon[4], Gregory H. Bird[10,11], Hyuk-Soo Seo[1,12], Sirano Dhe-Paganon[1,12], Jurre J. Kamphorst[9], Andrew F. Stewart[3], A. M. James Shapiro[5], Jarrod A. Marto[1,6,7,8], Loren D. Walensky[10,11], Russell G. Jones[13], Adolfo Garcia-Ocana[3] and Nika N. Danial[1,14,15] ✉

Chronic inflammation is linked to diverse disease processes, but the intrinsic mechanisms that determine cellular sensitivity to inflammation are incompletely understood. Here, we show the contribution of glucose metabolism to inflammation-induced changes in the survival of pancreatic islet β-cells. Using metabolomic, biochemical and functional analyses, we investigate the protective versus non-protective effects of glucose in the presence of pro-inflammatory cytokines. When protective, glucose metabolism augments anaplerotic input into the TCA cycle via pyruvate carboxylase (PC) activity, leading to increased aspartate levels. This metabolic mechanism supports the argininosuccinate shunt, which fuels ureagenesis from arginine and conversely diminishes arginine utilization for production of nitric oxide (NO), a chief mediator of inflammatory cytotoxicity. Activation of the PC–urea cycle axis is sufficient to suppress NO synthesis and shield cells from death in the context of inflammation and other stress paradigms. Overall, these studies uncover a previously unappreciated link between glucose metabolism and arginine-utilizing pathways via PC-directed ureagenesis as a protective mechanism.

Glucose imparts protective or detrimental effects in a range of cell types depending on the extent and duration of the increase in glucose flux[1–4]. An example of this is the intricate context- and dose-dependent modulatory effects of glucose on the survival of insulin-producing β-cells. In particular, prolonged exposure to high glucose impairs β-cell survival and function cooperatively with inflammation in diabetes and obesity[1,5–7]. Although important advances have been made in understanding the immune-cell component of inflammation in these pathologies[6,8–10], the cell-intrinsic biochemical connection between glucose metabolism and the response of target cells to inflammation has not been defined.

Results

The effect of glucose metabolism on the survival of human islets undergoing inflammation. To dissect the molecular effectors of glucose metabolism that control β-cell viability in the context of inflammation, we treated human donor islets with a combination of proinflammatory cytokines (tumour necrosis factor-α (TNF-α), interleukin-1β (IL-1β) and interferon-γ (IFN-γ)), shown to mimic β-cell inflammation in diabetes[6,7]. In this system, we examined how increased glucose metabolism via activation of glucokinase (GK, hexokinase IV), the hexokinase isoform expressed in these cells[11], influences inflammation-induced cell death and whether the protective versus non-protective effects of glucose can be distinguished. We have previously shown that GK activation via phosphorylation of the GK-binding protein BAD preserves β-cell survival in response to a variety of stress signals, including inflammatory cytokines[12]. This prompted investigation into whether other established modes of GK activation could be similarly protective. GK activation at its allosteric site by gain-of-function mutations identified in humans with hyperinsulinemic hypoglycaemia (for example, GK Y214C[13]), or by small molecule allosteric GK activators[11] (GKAs, for example, RO0281675 (ref. [14])), substantially augments the enzyme's affinity for glucose[11,15], but does not protect human islets from cytokine-induced death (Fig. 1a–c and Extended Data Fig. 1a–c). In contrast, GK activation near its active site by mimicking BAD phosphorylation using either the phosphomimic mutant of BAD within its BCL-2 homology 3 (BH3) α-helix (BAD SD), or hydrocarbon stapled peptides modelled after the phospho-BAD BH3 helix (BAD $SAHB_A$ SD)[12,16–18], maintains GK's native affinity for glucose[18] and spares human islets from inflammation-induced death (Fig. 1a–c and Extended Data Fig. 1a–e). This protective effect requires the GK-activating capacity of phospho-BAD because a BAD BH3 mutant harboring triple-alanine substitutions that does not bind or activate GK, BAD AAA[12,19], or the corresponding

[1]Department of Cancer Biology, Dana-Farber Cancer Institute, Boston, MA, USA. [2]Department of Cell Biology, Harvard Medical School, Boston, MA, USA. [3]Diabetes, Obesity and Metabolism Institute, Department of Medicine, Division of Endocrinology, Diabetes and Bone Disease, Icahn School of Medicine at Mount Sinai, New York, NY, USA. [4]Rosalind and Morris Goodman Cancer Center Metabolomics Core, Montreal, Canada. [5]Clinical Islet Transplant Program, Department of Surgery, University of Alberta, Edmonton, Canada. [6]Blais Proteomics Center, Dana-Farber Cancer Institute, Boston, MA, USA. [7]Department of Oncologic Pathology, Dana-Farber Cancer Institute, Boston, MA, USA. [8]Department of Pathology, Brigham and Women's Hospital, Harvard Medical School, Boston, MA, USA. [9]Rheos Medicines, Cambridge, MA, USA. [10]Department of Pediatric Oncology, Dana-Farber Cancer Institute, Boston, MA, USA. [11]Linde Program in Cancer Chemical Biology, Dana-Farber Cancer Institute, Boston, MA, USA. [12]Department of Biological Chemistry and Molecular Pharmacology, Harvard Medical School, Boston, MA, USA. [13]Metabolic and Nutritional Programming, Center for Cancer and Cell Biology, Van Andel Institute, Grand Rapids, MI, USA. [14]Department of Medical Oncology, Dana-Farber Cancer Institute, Boston, MA, USA. [15]Department of Medicine, Harvard Medical School, Boston, MA, USA. ✉e-mail: nika_danial@dfci.harvard.edu

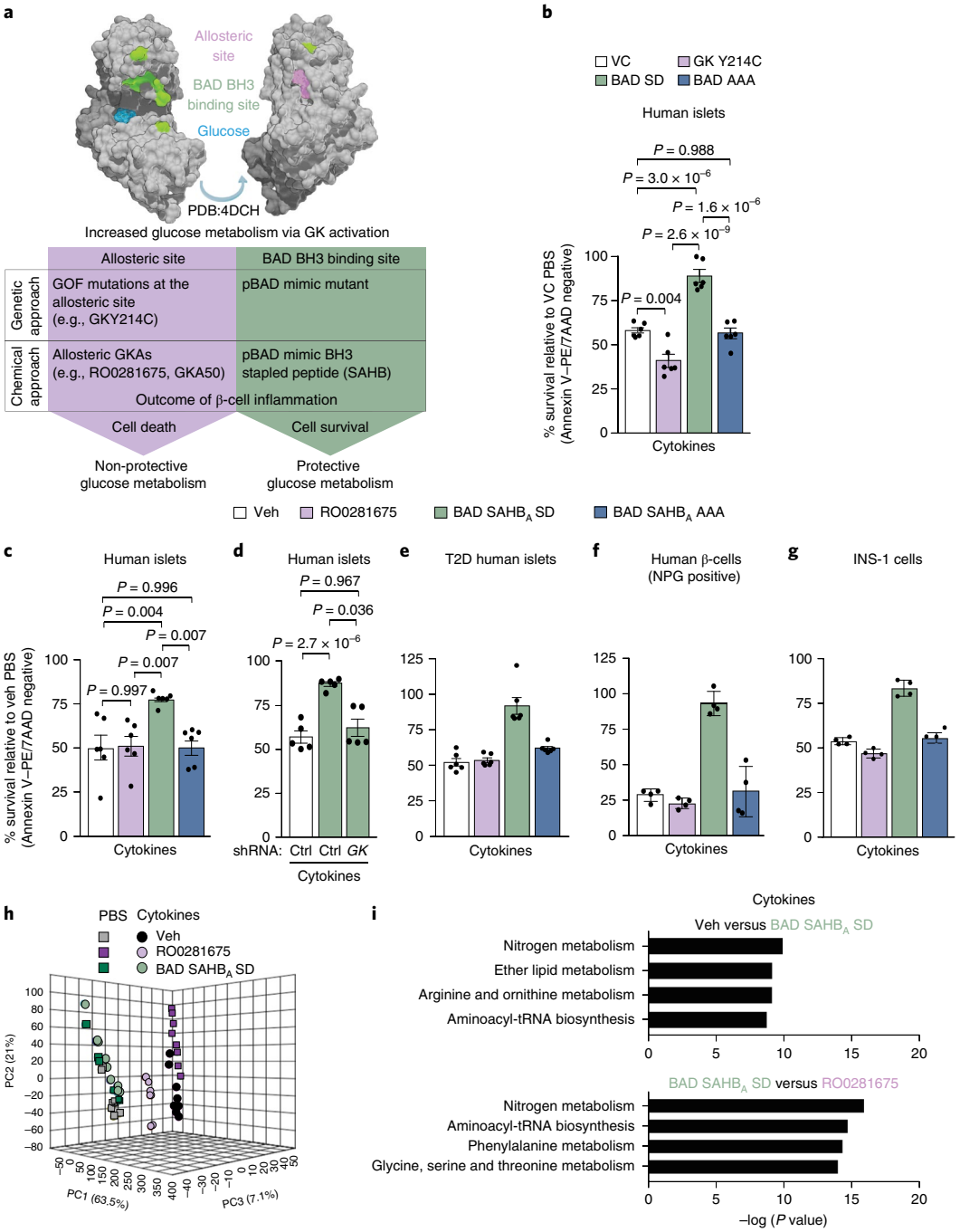

Fig. 1 | Protective versus non-protective glucose metabolism in human islets undergoing inflammation and attendant metabolite signatures. **a**, Schematic summary showing modelling of protective versus non-protective glucose metabolism using GK-targeted genetic and pharmacologic tools. GOF, gain of function. PDB: 4DCH. **b**, Viability of human islets expressing vector control (VC), GK Y214C, BAD SD or BAD AAA following 48 h of treatment with a cocktail of inflammatory cytokines (TNF-α, IL-1β and IFN-γ). Values are normalized to results from VC PBS control treatment. Data are from $n = 3$ human donors each with 2 replicates. **c**, Viability of human islets treated with vehicle (Veh, DMSO), RO0281675, BAD $SAHB_A$ SD or BAD $SAHB_A$ AAA and exposed to cytokines for 48 h as in **b**, $n = 6$ donors. **d**, Viability of human islets subjected to *GK* knockdown and treated with vehicle or BAD $SAHB_A$ SD in the presence of inflammatory cytokines. Data are from $n = 5$ independent experiments using islet cultures from 2 donors. **e**, Viability of T2D donor islets treated as in **c**. Data are from $n = 2$ independent experiments using islet cultures from 2 donors. **f**, Viability of β-cells within human islets treated as in **c** and visualized by co-staining with Newport green and phycoerythrin (PE)-conjugated Annexin V with 7AAD. Data are means ± s.d. from $n = 4$ technical replicates of islets cultures from one donor. **g**, Viability of INS-1 β-cells treated as in **c**. Data are means ± s.d. from $n = 4$ technical replicates. **h**, Principal component analysis (PCA) of LC–MS untargeted metabolomics of human islets treated as in **c** for 24 h, n = 5 donors pooled and split into 8 replicates for metabolomics analysis. **i**, Pathway analysis displayed as bar plot showing pathway –log (*P* values), revealing nitrogen, arginine and ornithine metabolism as the top pathways changed in vehicle control versus BAD $SAHB_A$ SD or in RO0281675 versus BAD $SAHB_A$ SD comparisons, $n = 5$ donors. For RO0281675 versus BAD $SAHB_A$ SD comparisons, arginine and ornithine metabolism is not displayed but is statistically enriched with a *P* value of 1.21×10^{-8}. Data in **b**–**d** and **i** are means ± s.e.m. with statistical analyses on means from independent experiments using one-way analysis of variance (ANOVA) with Tukey adjustment for multiple comparisons.

BAD BH3 stapled peptide (BAD SAHB$_A$ AAA)[12,16] is not protective under similar settings (Fig. 1b,c and Extended Data Fig. 1a,c,d). Importantly, the pro-survival benefit of BAD SAHB$_A$ SD in human islets is abolished upon *GK* knockdown (Fig. 1d and Extended Data Fig. 1f), indicating that protection by phospho-BAD mimicry is GK-dependent and on-target. These two independent modes of GK activation (allosteric site activation and phospho-BAD mimicry) essentially establish a system in which we can model the protective versus non-protective outcomes of increased glucose metabolism to identify the specific metabolic pathways downstream of glucose that determine cell survival during inflammation (Fig. 1a).

We next tested this modelling of protective versus non-protective glucose metabolism in a few additional settings. We found that the protective effect of phospho-BAD mimicry is also observed in type 2 diabetes (T2D) donor islets treated with inflammatory cytokines, and markedly contrasts with the non-protective outcome of GK activation at its allosteric site (Fig. 1e). Because human islets comprise ~40–60% β-cells out of the total of multiple islet cell types, we further verified that the above findings in whole islets demonstrate genuine β-cell survival differences by quantifying viability of cells positive for Newport Green, which stains insulin granules found only in β-cells (Fig. 1f). In addition, the contrasting effects of these GK-activating modalities on sensitivity/resistance to inflammation-induced death is reproducible in the INS-1 β-cell line (Fig. 1g).

Changes in arginine metabolism differentiate protective and non-protective GK activation. The above data indicate that we can effectively model non-protective versus protective outcomes of increased glucose metabolism in β-cells using complimentary genetic and pharmacologic GK-activating tools (Fig. 1a). We then used this system as a discovery platform to learn about the metabolic mechanism whereby glucose determines cell survival during inflammation. To this end, we undertook non-targeted metabolomics to compare the broad metabolite signatures of human donor islets in the absence (PBS) or presence of inflammatory cytokines following treatment with GKA RO0281675 or BAD SAHB$_A$ SD, herein referred to as non-protective or protective GK activation/glucose metabolism, respectively. The largest differences across conditions were observed in the presence of cytokines (Fig. 1h and Extended Data Fig. 2), and subsequent topological analyses using the Kyoto Encyclopedia of Genes and Genomes (KEGG) pathway database identified nitrogen ($P = 9.3 \times 10^{-9}$), arginine and ornithine metabolism ($P = 5.2 \times 10^{-8}$) among the top pathways significantly differentiating the metabolic profiles of protective glucose metabolism via BAD SAHB$_A$ SD- from vehicle (DMSO), and from RO0281675-treated islets (nitrogen; $P = 9.4 \times 10^{-15}$, arginine and ornithine metabolism; $P = 6.6 \times 10^{-8}$) (Fig. 1i). Secondary validation using targeted liquid chromatography–tandem mass spectrometry (LC–MS/MS) analysis of human islets from five additional donors confirmed these findings. This prompted focused examination of arginine-utilizing pathways (Fig. 2a), which revealed a remarkable difference in urea and NO accumulation in that protective glucose metabolism augments urea levels while diminishing NO in the presence of cytokines (Fig. 2b and Extended Data Fig. 3a). These differences were further recapitulated with a second, structurally distinct allosteric GKA, GKA50 (ref. [20]) (Fig. 2c and Extended Data Fig. 3b). Importantly, *GK* depletion in human islets abolished the effects of phospho-BAD mimicry on urea and NO, underscoring GK's role in this setting and pointing to a link between glucose metabolism and arginine-utilizing pathways (Fig. 2d). The differential effect of protective versus non-protective GK activation on urea and NO levels also holds in the INS-1 β-cell line (Fig. 2e). Importantly, the urea-enhancing and NO-reducing outcomes of protective glucose metabolism are also evident in human islets expressing the full-length BAD SD protein in comparison with the GK Y214C gain-of-function mutant at the allosteric site (Fig. 2f and Extended Data Fig. 3c). Thus, the metabolic features distinguishing non-protective versus protective glucose metabolism are not limited to pharmacologic GK activation and are identical when using genetic tools to activate GK through these two distinct mechanisms (Fig. 1a). Of note, islets expressing the non-GK-activating full-length BAD AAA mutant[12,19] showed levels of urea and NO that were comparable to those in vector control (VC)- or GK Y214C-expressing islets (Fig. 2f and Extended Data Fig. 3c). Similarly, the BAD BH3 stapled peptides modelled after the BAD AAA mutant (BAD SAHB$_A$ AAA) did not enhance urea or reduce NO levels in the presence of inflammatory cytokines compared with vehicle or RO0281675 (Fig. 2e). These important controls underscore the specificity of both the genetic and chemical tools used to experimentally model and distinguish between features of protective versus non-protective glucose metabolism.

Protective glucose metabolism directs arginine to the urea cycle in human islets. Ureagenesis has not been extensively examined in β-cells. In our studies, the urea levels produced by islets (8–20 μM) are three orders of magnitude lower than normal circulating urea levels in humans (2–7 mM), or pathologic concentrations (~20 mM) shown to impair β-cell function, as in chronic kidney disease[21]. We confirmed the expression of many urea cycle enzymes and associated pathways in this cell type by subjecting fluorescence-activated cell sorting (FACS)-purified human β-cells to proteomic and RNA sequencing (RNA-seq) analyses (Fig. 3a,b, Extended Data Fig. 4 and Supplementary Table 1), as well as immunostaining fresh islet preparations for these enzymes within the insulin-positive β-cell compartment (Fig. 3c). To biochemically quantify the reactions relevant for the synthesis of urea and NO via arginase (ARG) and nitric oxide synthase (NOS) enzymes, respectively, we used the L-[guanidino-$^{15}N_2$]arginine tracer. Labelling of human islets revealed protective glucose metabolism is associated with higher enrichment of $^{15}N_2$ in urea (M+2) and lower citrulline (M+1) synthesis, indicative of diminished NO synthesis (BAD SAHB$_A$ SD, Fig. 3d,e). In contrast, ureagenesis was not altered in control samples (Veh and BAD SAHB$_A$ AAA, Fig. 3d), or following non-protective GK activation (RO0281675, Fig. 3d). We did not detect any differences in the expression of iNOS or arginase 2 (ARG2), the main NOS and ARG isoforms in human β-cells[22]. As such, differential urea and NO synthesis in this setting is more likely to be due to substrate-driven differences in enzyme activity. Importantly, treatment with the arginase inhibitor ABH (2(S)-amino-6-boronohexanoic acid) abrogates the protective effect of GK activation in islets undergoing inflammatory stress (Fig. 3f). Overall, these data indicate that protective glucose metabolism engages ureagenesis in the face of inflammation, which is commensurate with diminished NO accumulation.

Protective glucose metabolism links aspartate to the urea cycle to counter inflammation. The above findings prompted investigation of the specific link between glucose and arginine metabolism that could explain how protective glucose metabolism would lead to increased urea cycle activity. Aspartate is required for the production of the rate-limiting urea cycle substrate argininosuccinate, and is a potential metabolic node for modulation by glucose. Glucose carbons can contribute to aspartate pools via the tricarboxylic acid (TCA) cycle metabolite oxaloacetate (OAA) (Fig. 4a). Thus, aspartate may link glucose to the urea cycle. We found that total aspartate levels were reduced in human islets treated with inflammatory cytokines and were further exacerbated by non-protective GK activation via RO0281675 (Fig. 4b). In contrast, aspartate pools remained stable in BAD SAHB$_A$ SD-treated islets in the absence or presence of cytokines (Fig. 4b). [$^{13}C_6$]glucose tracer analyses provided direct evidence that protective GK activation supports a higher incorporation of glucose carbons into aspartate in the

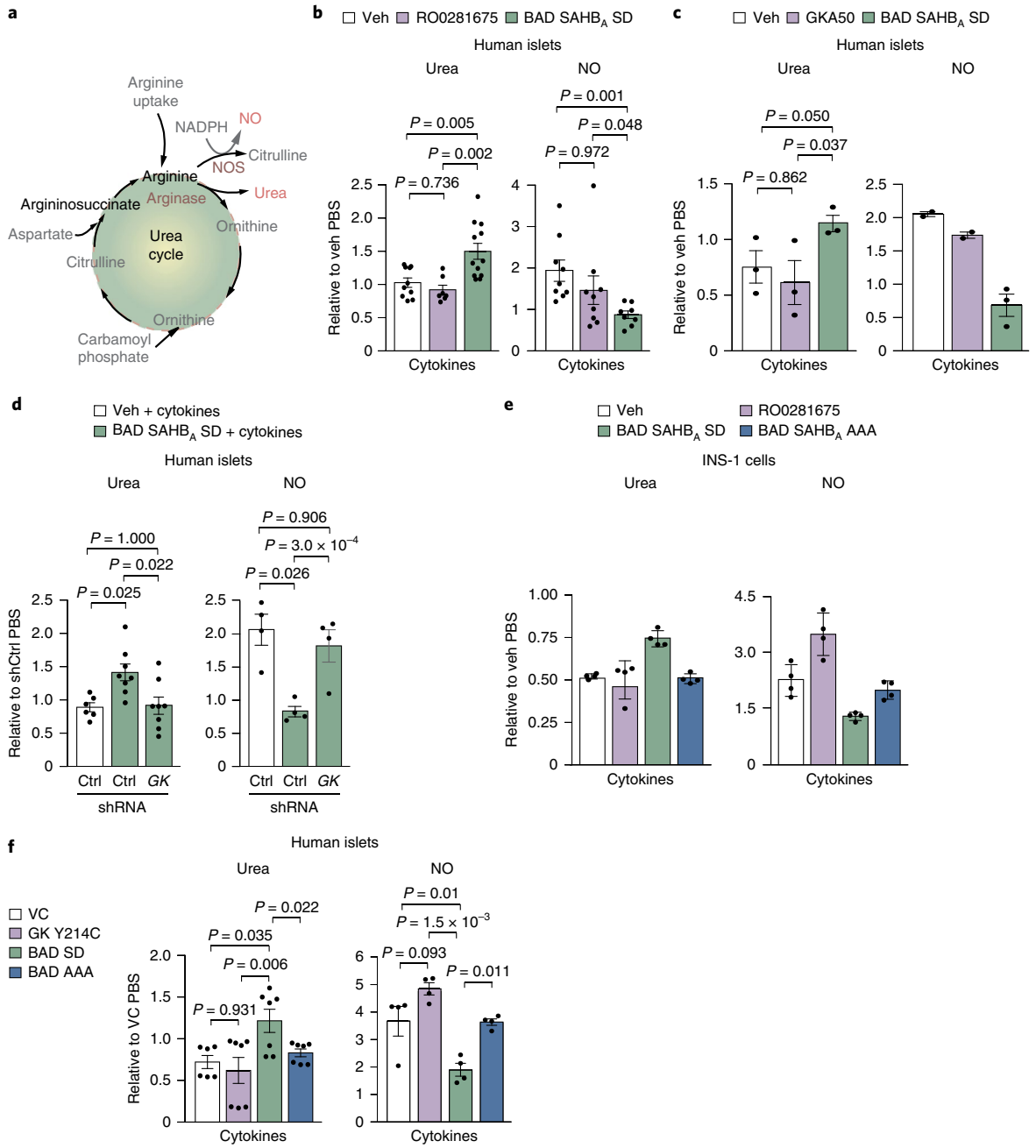

Fig. 2 | Differential modulation of arginine metabolism by protective versus non-protective GK activation in human islets. a, Schematic of arginine usage for urea and NO synthesis. **b**, Quantification of urea and NO levels in human islets treated with the indicated compounds and exposed to cytokines for 24 h. Values are shown relative to vehicle control PBS samples. Data for urea are from $n=10$ (Veh), $n=7$ (RO0281675) and $n=12$ (BAD SAHB$_A$ SD) human donors. Data for NO are from $n=9$ (Veh and RO0281675) and $n=8$ (BAD SAHB$_A$ SD) human donors. **c**, Quantification of urea and NO in human islets treated with the indicated compounds and exposed to inflammatory cytokines as in **b**. Data for urea are from $n=3$ donors. Data for NO are from $n=2$ (Veh and GKA50) and $n=3$ (BAD SAHB$_A$ SD) donors. **d**, Urea and NO levels in *GK*-depleted human islets treated with BAD SAHB$_A$ SD and cytokines as in **b**. Data for urea are from $n=4$ independent experiments using islet cultures from 2 donors. Data for NO are from $n=4$ donors. **e**, Urea and NO levels in INS-1 cells treated as in **b**, measured at 24 h. Data are means ± s.d. of $n=4$ technical replicates. **f**, Urea and NO levels in human islet expressing the indicated GK and BAD mutants and treated with cytokines as in (b). Data for urea are from 6 (VC) and 7 (GK Y214C, BAD SD and BAD AAA) replicates using islet cultures from 2 donors performed over $n=4$ independent experiments. Data for NO are from $n=4$ independent experiments using islet cultures from 2 donors. Data in **b**–**d** and **f** are means ± s.e.m. with statistical analyses on means from independent experiments using one-way ANOVA with Tukey adjustment for multiple comparisons (**b**–**d**) and Fisher's exact test (**f**).

presence of inflammatory cytokines, in contrast to non-protective GK activation at the allosteric site (Fig. 4c and Extended Data Fig. 5a). A role for aspartate in glucose-stimulated ureagenesis stipulates that it would contribute to argininosuccinate synthesis, which would in turn depend on the activity of GOT1/2 aspartate aminotransferases catalysing aspartate synthesis from glucose-derived OAA (Fig. 4a). Indeed, knockdown of either *GOT1* or *GOT2* using multiple different short hairpin RNAs (shRNAs) diminished urea levels along with aspartate (Fig. 4d and Extended Data Fig. 5b–d). GOT1/2 depletion also led to elevated NO levels and reduced the viability of

BAD $SAHB_A$ SD-treated islets (Fig. 4d,e and Extended Data Fig. 5d). These results point to a protective ureagenic outcome of GOT1/2 activity, congruent with the idea that aspartate produced by these aminotransferases can support argininosuccinate (AS) synthesis to fuel the urea cycle. Consistent with this notion, AS supplementation is sufficient to increase urea levels and rescue the viability of human islets undergoing inflammation (Fig. 4f–g). Taken together, our data provide support for a previously unappreciated link between glucose and the urea cycle, and suggest that this metabolic mechanism of preserving aspartate pools reduces NO synthesis and shields cells from the cytotoxic effects of inflammation.

Pyruvate carboxylase mediates the protective outcomes of glucose and arginine metabolism. We next investigated the source of the increased aspartate following protective GK activation by determining which other metabolites contained isotopically labelled carbon from [$^{13}C_6$]glucose in islets undergoing inflammatory stress. Malate M+3 was increased, whereas citrate M+2 was unchanged (BAD $SAHB_A$ SD, Fig. 5a and Extended Data Fig. 6a). We interpret such labelling patterns as an increase in PC activity (M+3 malate), no change in pyruvate dehydrogenase (PDH) activity (M+2 citrate) and higher PC to PDH activity ratio (Extended Data Fig. 6b). Independent biochemical measurements provided corroborative evidence that PC activity is higher in cytokine-treated human islets following protective versus non-protective GK activation (Extended Data Fig. 6c). We next tested whether PC is relevant for the protective partitioning of arginine to the urea cycle away from utilization by NOS. *PC* knockdown in human islets undergoing inflammatory stress blunts the urea-enhancing and NO-reducing capacity of protective glucose metabolism concomitant with a significant reduction in aspartate levels (Fig. 5b,c and Extended Data Fig. 6d, lanes 1 versus 3). Moreover, on-target, shRNA-mediated depletion of *PC* or chemical inhibition of this enzyme using phenyl acetic acid (PAA) blocked the pro-survival benefits of GK activation (Fig. 5d,e and Extended Data Fig. 6d). Remarkably, the requirement for PC in augmenting urea and promoting survival in this setting is not recapitulated by glutaminase (GLS), another anaplerotic enzyme that could serve as a potential source of aspartate for argininosuccinate synthesis (Fig. 4a). Specifically, chemical inhibition of GLS did not interfere with urea levels or the pro-survival effects of protective glucose metabolism (Fig. 5f and Extended Data Fig. 6e). Taken together, these findings are intriguing from both mechanistic and conceptual standpoints in that they establish a previously unexplored link between mitochondrial pyruvate handling via PC and arginine utilization through the ARG reaction. This mechanism restrains inflammation-induced augmentation of NO production and reveals an anti-inflammatory role for glucose metabolism via regulation of the urea cycle.

PC-dependent effects of protective glucose metabolism on islets and diabetes reversal. The prominence of PC in the above in vitro assays warranted investigation of its relevance in long-term β-cell protective outcomes of GK activation in vivo. To this end, we used a model of marginal-mass islet transplantation. Islet transplantation in both humans and rodent models can have limited efficacy due, in part, to islet graft inflammation. Specifically, local production of cytokines at the site of engraftment and the presence of cytokines in the sera of islet-transplant recipients have been reported[23]. We found that protective activation of GK in human donor islets prior to transplantation reduced β-cell death in islet grafts as early as day 2 post transplantation, and reversed hyperglycaemia in diabetic mice over time, while non-protective GK activation or control treatments were ineffective (BAD $SAHB_A$ SD versus RO0281675, BAD $SAHB_A$ AAA or vehicle control, Fig. 6a,b, Table 1 and Supplementary Tables 2 and 3). The superior engraftment and physiologic functionality of protected islets was also evident from their ability to replenish insulin levels upon engraftment in vivo and from improved glucose clearance during a glucose-tolerance test (GTT) (Fig. 6c,d). Importantly, chemical inhibition of PC with PAA in BAD $SAHB_A$ SD-treated donor islets blocked the efficiency of islet engraftment and systemic improvement in glucose homeostasis (Fig. 6a–d, Table 1 and Supplementary Tables 2 and 3). These data underscore the functional relevance of PC as a downstream mediator of protective glucose metabolism in islets.

PC-directed ureagenesis protects human islets from inflammation and glucotoxicity. While we originally arrived at the connection between PC and arginine metabolism by modelling glucoprotection or lack thereof through different modes of GK activation, additional studies indicated that this metabolic link is itself a protective mechanism and is not restricted to experimental modulation of GK. Specifically, overexpression of PC in human islets augments urea, diminishes NO and protects from inflammation-induced death independent of any genetic or pharmacologic modulation of GK, and effectively phenocopies the outcome of ARG2 overexpression on these same parameters (Fig. 7a,b and Extended Data Fig. 7a). Conversely, PC depletion alone is sufficient to reduce ureagenesis from arginine and enhance NO levels in cytokine-treated human islets (Fig. 7c and Extended Data Fig. 7b). The ability of PC to fuel ureagenesis suggests that this TCA cycle enzyme prevents the aspartate–argininosuccinate shunt from becoming limited for urea cycle activity in the presence of pro-inflammatory cytokines. Consistent with this notion, AS supplementation of PC-depleted

Fig. 3 | Protective glucose metabolism directs arginine to the urea cycle away from NO synthesis in islets undergoing inflammation. a, Histogram of relative abundance of 3,160 proteins detected (out of 5,399 total, see Supplementary Table 1) by LC–MS/MS in 8.7×10^4 purified human β-cells from $n=3$ human donors. Green lines indicate gene products related to the urea cycle, argininosuccinate and aspartate metabolism detected at the protein level. **b**, Expression levels of genes related to the urea cycle, pyruvate metabolism and arigninosuccinate shunt, based on RNA-seq analysis of FACS-sorted human β-cells from $n=3$ donors; data are in $\log_2$(counts per million bases). **c**, Co-immunostaining of insulin and individual metabolic enzymes related to the urea cycle in dispersed human islet cells from one donor representing similar results obtained from two additional donors. Representative images are shown (left). Scale bar, 10 μm. Mean fluorescence intensity (FI) within the insulin-positive region of interest (ROI) was calculated from five images per antibody (right). Neg denotes negative control for background Alexa Fluor 488 signal with insulin co-stain. Statistical analyses are Student's *t*-tests of each enzyme compared with neg. ASL, argininosuccinate lyase; ASS1, argininosuccinate synthase 1; CPS1, carbamoyl-phosphate synthase 1; DDAH1, dimethylarginine dimethylaminohydrolase 1; DDAH2, dimethylarginine dimethylaminohydrolase 2; GOT1, aspartate aminotransferase 1; GOT2, aspartate aminotransferase 2; MDH1, malate dehydrogenase 1; MDH2, malate dehydrogenase 2; NAGS, *N*-acetyl-glutamate synthase; OAT, ornithine aminotransferase; SLC25A12, solute carrier family 25 member 12/calcium-binding mitochondrial carrier protein Aralar 1; SLC25A13, solute carrier family 25 member 13/calcium-binding mitochondrial carrier protein Aralar 2; SLC25A15, solute carrier family 25 member 15/mitochondrial ornithine transporter 1. **d**,**e**, Cytokine-induced changes in the partitioning of L-[$^{15}N_2$]arginine to urea (**d**) and citrulline/NO (**e**) synthesis in human islets, comparing protective versus non-protective glucose metabolism as modelled by BAD $SAHB_A$ SD versus RO0281675 treatment, respectively; $n=4$ donors. **f**, Chemical inhibition of arginase via ABH interferes with the protective effect of BAD $SAHB_A$ SD in human islets undergoing inflammation, $n=5$ donors. Data are means ± s.e.m. with one-way (**d**,**e**) and two-way (**f**) ANOVA statistical tests with Tukey adjustment for multiple comparisons.

cells rescues urea levels and protects against inflammation toxicity (Fig. 7d,e). This suggests that supplying the urea cycle with substrate is sufficient to enhance ureagenesis when flux through PC is constricted and PC-derived aspartate is limiting. Taken together, the above combination of gain- and loss-of-function studies and metabolite-supplementation experiments indicate that arginine utilization through the ARG and NOS routes is acutely modulated by PC activity, and are consistent with a link between mitochondrial pyruvate handling and the urea cycle via the aspartate–argininosuccinate shunt.

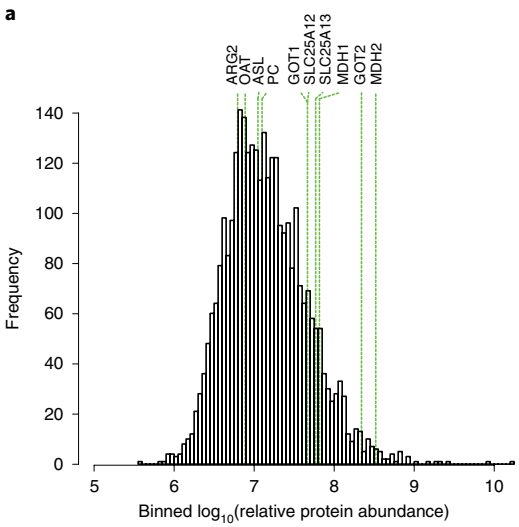

b

Expression of urea cycle enzymes and related pathways based on RNA-seq analysis of sorted human β-cells

Gene	Donor 1	Donor 2	Donor 3
PC	3.54	3.52	3.37
MDH2	8.36	9.89	7.96
GOT1	5.70	6.66	5.19
CPS1	0.28	0.18	0.61
ARG2	3.99	4.40	4.04
ASS1	4.07	5.10	4.27
ASL	4.07	4.31	3.52
OAT	5.84	6.47	5.75
GOT2	6.40	7.16	6.04
NAGS	1.76	2.71	2.59
MDH1	7.39	8.57	7.11
SLC25A15	1.68	1.64	1.88
SLC25A13	6.11	6.00	6.03
SLC25A12	5.01	5.37	4.63

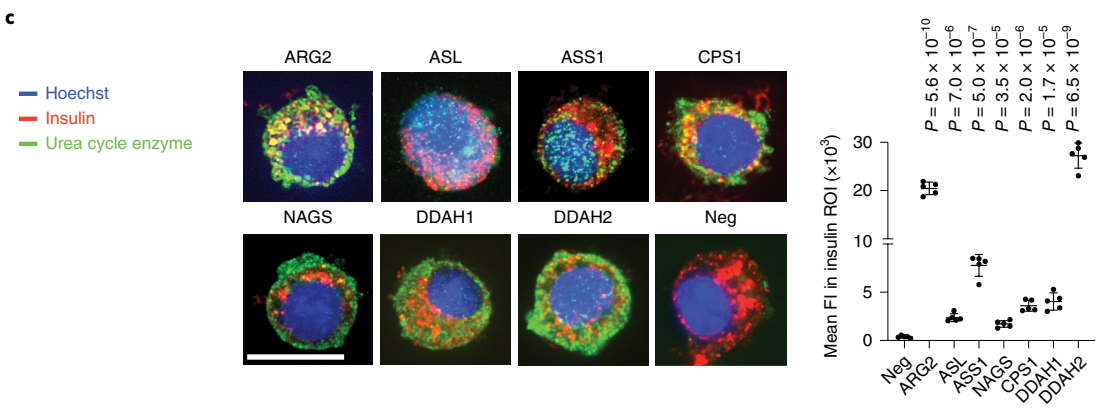

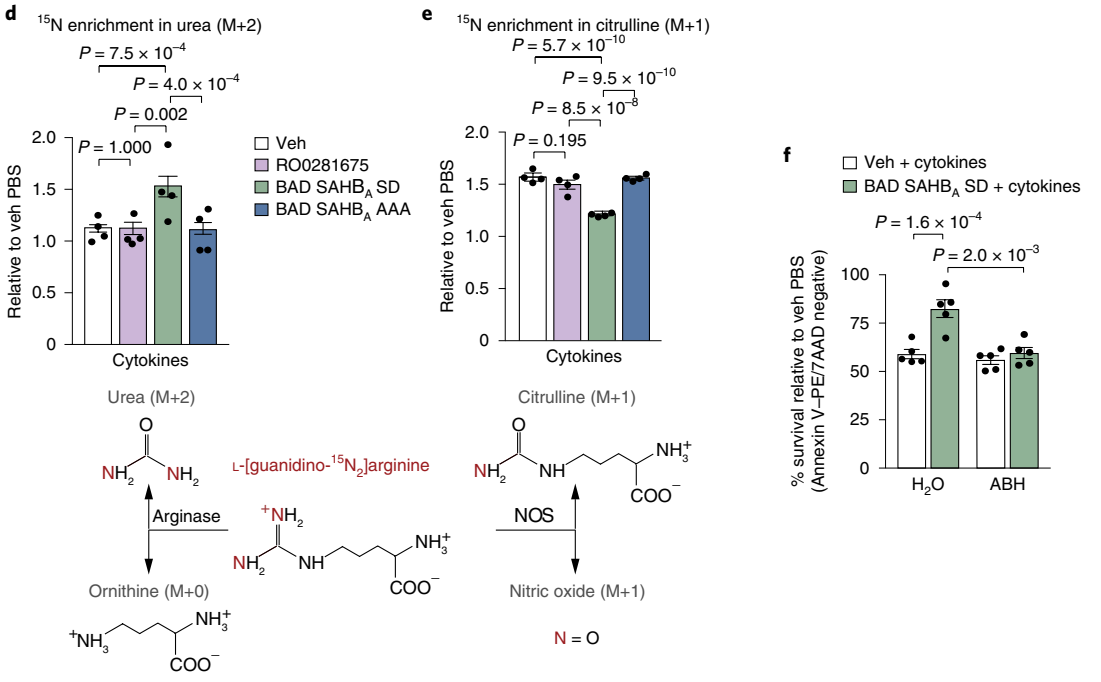

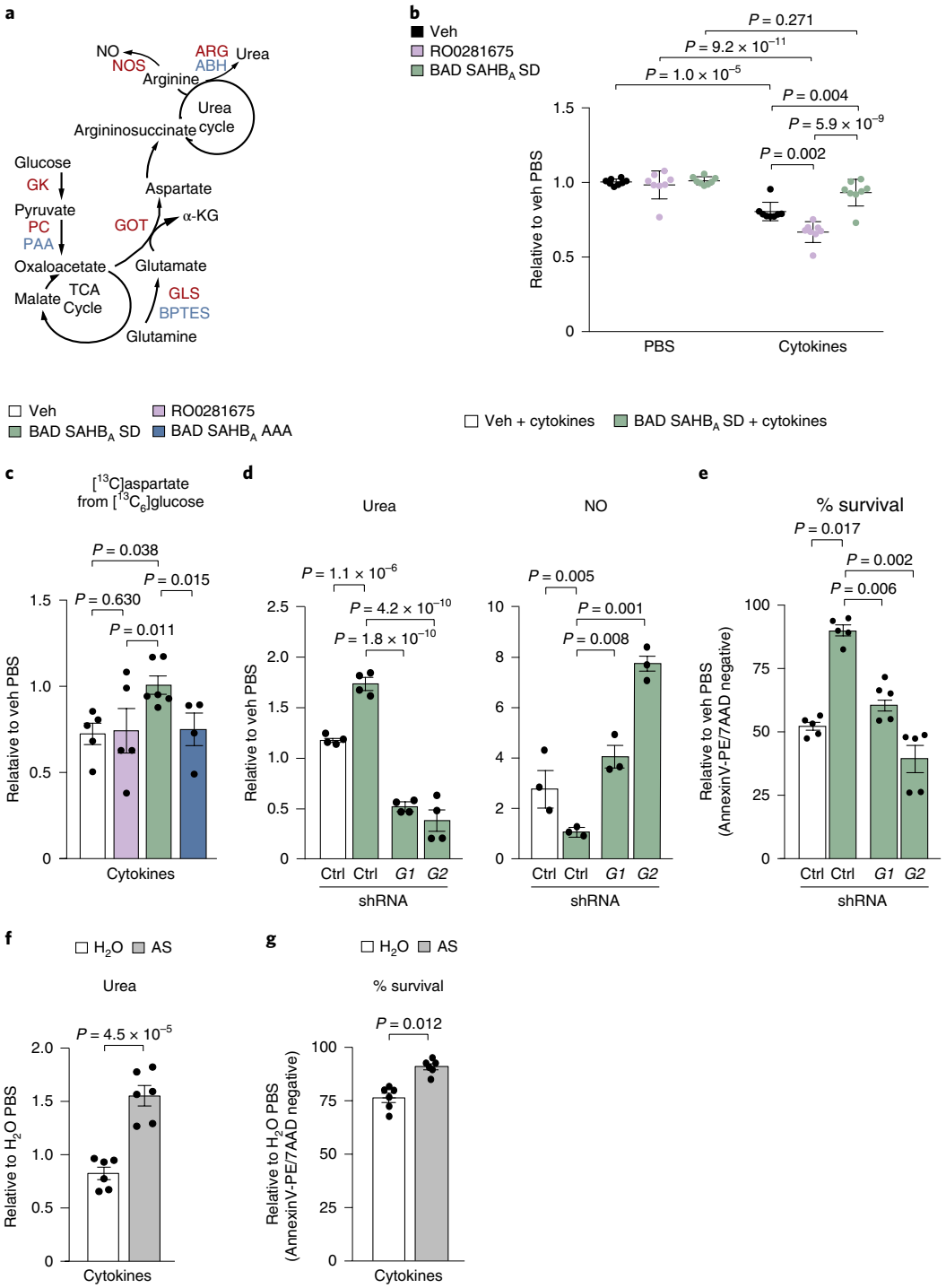

Fig. 4 | Protective glucose metabolism links aspartate to the urea cycle to counter inflammation. a, Schematic of the TCA and urea cycles and their connection via the aspartate–argininosuccinate shunt. Enzymes of interest are marked in red and their corresponding inhibitors in blue**. b**, Total aspartate levels in human islets treated with the indicated compounds and cultured in the absence or presence of inflammatory cytokines. Data are from the untargeted metabolomics analysis in Fig. 1h, $n = 5$ human donors pooled and split into 8 replicates. **c**, Contribution of glucose to total aspartate pools in mouse islets labeled with [$^{13}C_6$]glucose and treated with inflammatory cytokines in the context of protective versus non-protective glucose metabolism. Data are from $n = 5$ (Veh, RO0281675), $n = 6$ (BAD SAHB$_A$ SD) and $n = 4$ (BAD SAHB$_A$ AAA) independent mouse islet isolations and experiments. See Extended Data Fig. 5a for isotopologue distribution of aspartate in an analogous labelling experiment. **d**,**e**, Quantification of urea and NO (**d**), and viability (**e**) in human islets subjected to shRNA-mediated *GOT1* (*G1*) or *GOT2* (*G2*) depletion and treated with cytokines in the context of protective versus non-protective glucose metabolism; $n = 4$ donors for urea, $n = 3$ donors for NO and $n = 5$ donors for viability measurements. Data for one hairpin per gene are displayed (sh1 for *GOT1* and sh2 for *GOT2*) from the full dataset of multiple hairpins (Extended Data Fig. 5b–d) **f**,**g**, Quantification of urea levels (**f**) and viability (**g**) in human islets supplemented with argininosuccinate (AS) in the presence of inflammatory cytokines, H_2O serves as vehicle control for AS. Data are from 6 independent experiments with $n = 3$ donors. Data are means ± s.e.m. with statistical analyses on means from independent experiments using one-way ANOVA with Tukey adjustment for multiple comparisons.

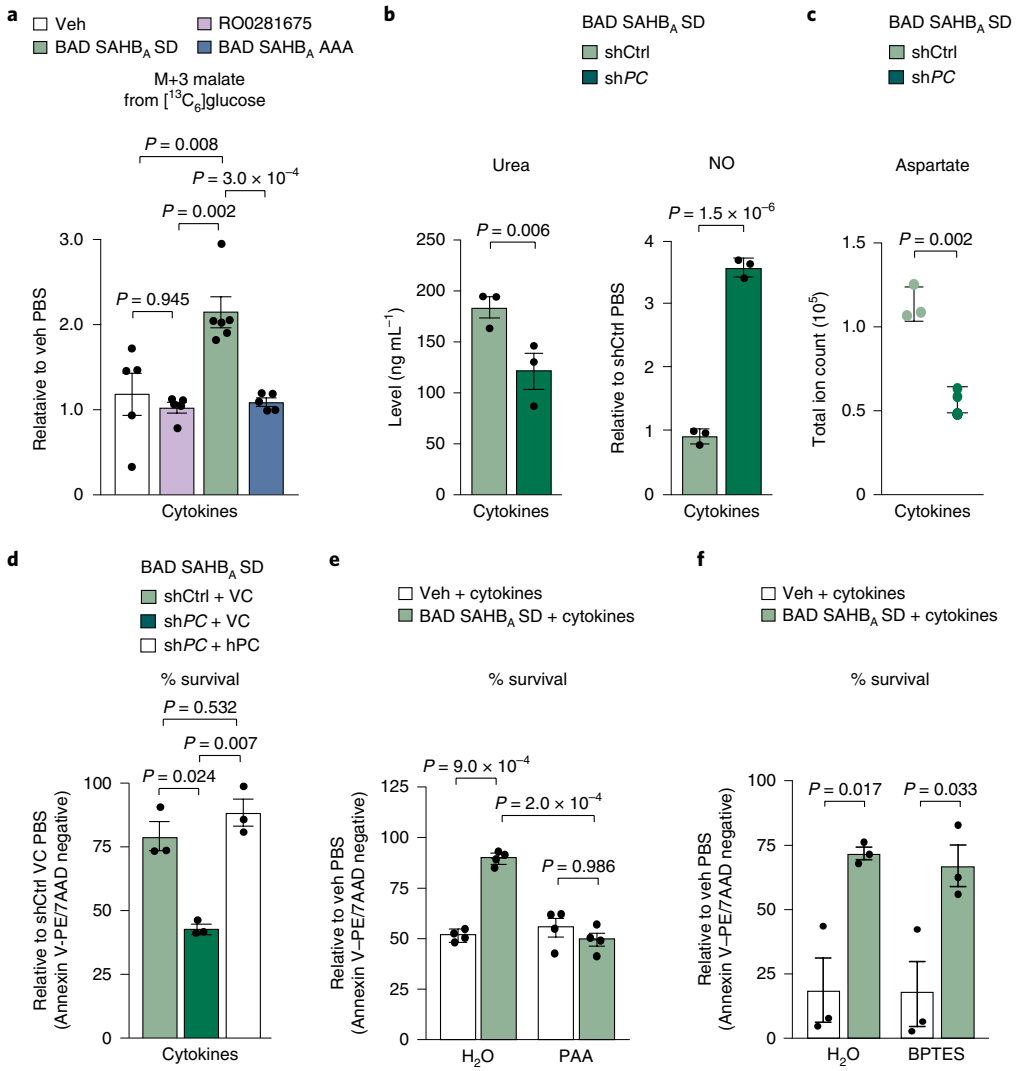

Fig. 5 | PC supports aspartate and ureagenesis, and is required for the protective effects of glucose metabolism. a, M+3 malate levels in mouse islets labelled with [$^{13}C_6$]glucose and treated as in Fig. 4c. Data are pooled means from $n=5$ (Veh, RO0281675), $n=6$ (BAD SAHB$_A$ SD) and $n=5$ (BAD SAHB$_A$ AAA) independent experiments. **b**,**c**, The effect of *PC* knockdown on urea and NO (**b**) and aspartate levels (**c**) in human islets treated with cytokines in the context of protective glucose metabolism; $n=3$ human donors in **b**, and $n=3$ independent experiments from 1 donor in **c**. **d**, The effect of *PC* knockdown on viability of human islets treated as in **b**. On-target effects of knockdown were validated by rescue with an shRNA-resistant human PC cDNA compared to vector control (VC); $n=3$ donors. **e**, The effect of PC inhibition by PAA on the viability of human islets treated with cytokines in the context of protective glucose metabolism; $n=4$ donors. **f**, GLS activity is not required for the protective effects of glucose metabolism. Viability of BAD SAHB$_A$ SD-treated human islets exposed to inflammatory cytokines in the absence or presence of BPTES; $n=3$ donors. Data are means ± s.e.m. from independent experiments with statistical analyses using one-way ANOVA with Tukey adjustment for multiple comparisons.

In parallel studies, we examined whether the protective outcome of the PC–ARG pathway is restricted to inflammatory stress or has broader relevance in the context of other physiologically relevant islet stress paradigms. Chronic exposure to high glucose (glucotoxicity) is another stress paradigm, that, along with inflammation, is known to impair β-cell survival in the diabetic milieu[24]. To our knowledge, the relevance of arginine metabolism in the context of glucotoxicity has not been examined. We found that chronic exposure of human islets to 33 mM glucose reduces urea and enhances NO levels compared to those under normal islet culture conditions at 5.8 mM glucose (Fig. 7f,g and VC in Fig. 7h). Remarkably, overexpression of PC or ARG2 reversed these effects and was sufficient to protect islet viability in this setting (Fig. 7g–i). Thus, similarly to inflammation, glucotoxicity is associated with diminished urea levels and NO accumulation, which can be countered by PC activity and routing of arginine to the urea cycle (Fig. 7g).

Discussion

Our studies identify urea cycle activation as part of a cell-intrinsic, anti-inflammatory pathway that can be fuelled by glucose via PC and the argininosuccinate shunt. This glucose-driven protective mechanism ultimately shifts the direction of arginine metabolism to ureagenesis, sparing cells from damaging NO accumulation. Diminishing NO production is known to mitigate cell death in the context of inflammation, but we are not aware of previous studies showing that glucose can influence this process by controlling arginine utilization. This further highlights the relevance of our findings from a conceptual standpoint. Moreover, we provide multiple gain- and loss-of-function studies that position PC as a mechanistic

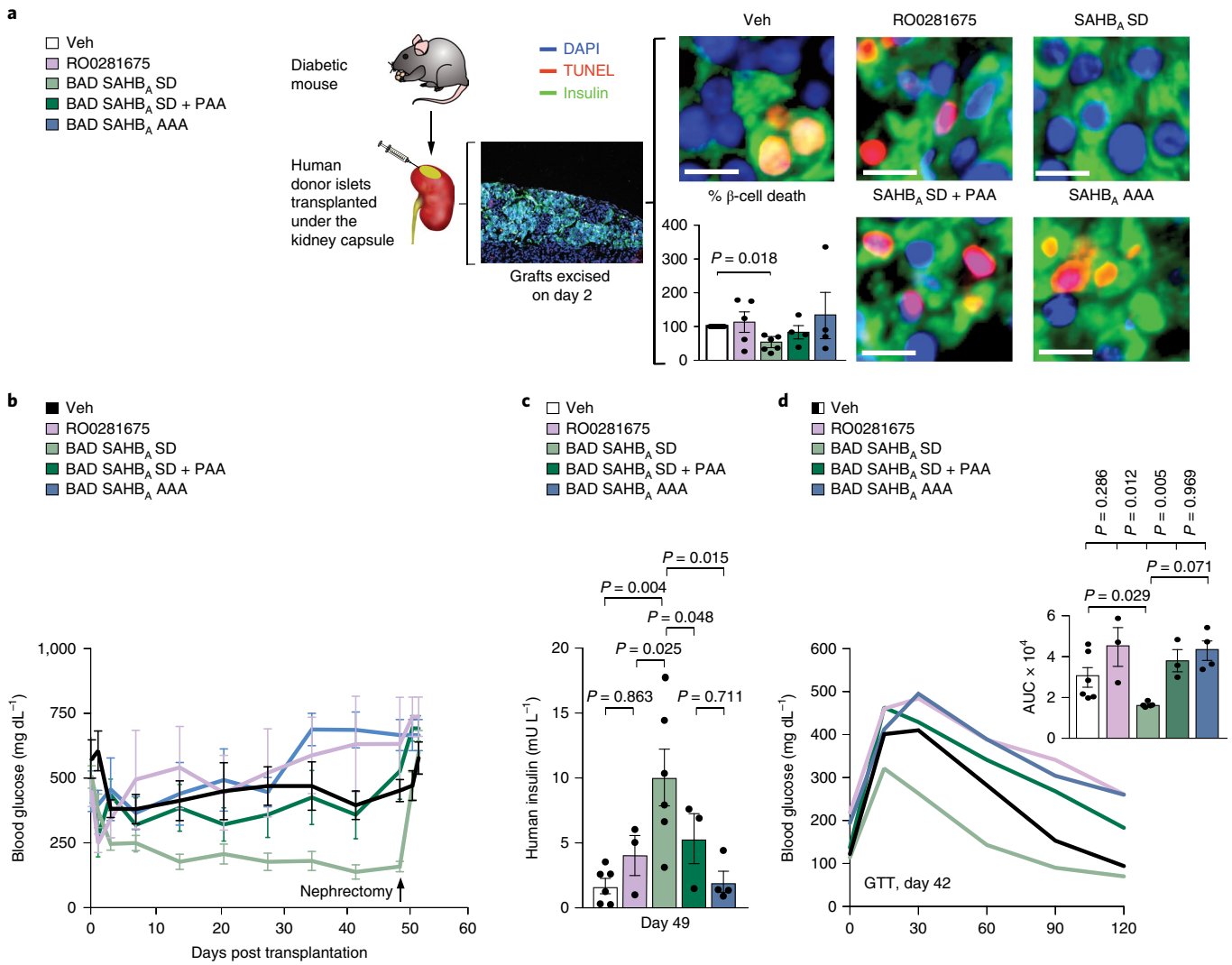

Fig. 6 | PC is required for the protective effects of glucose metabolism in human islets in vivo and their capacity to reverse diabetes in mice. **a**, Schematic of marginal-mass islet transplantation in diabetic NOD-SCID mice by using human donor islets pre-treated with the indicated single or double combination of compounds for 24 h prior to transplantation. Islet grafts were excised at day 2 post transplantation for quantification of β-cell death as the percentage of insulin- and TUNEL-double-positive cells with the *t*-test statistic. Representative images are shown. Scale bars, 10 μm. Data are from $n=6$ (Veh, BAD SAHB$_A$ SD), $n=5$ (RO0281675) and $n=4$ (BAD SAHB$_A$ SD + PAA, BAD SAHB$_A$ AAA) mice. **b**, Blood glucose levels of mice treated as in **a** measured up to 53 days post transplantation. Nephrectomy was performed at day 50 to excise grafts and show the requirement of protected donor islets for improving blood glucose. Statistical comparisons are provided in Table 1. Data are from $n=6$ (Veh, BAD SAHB$_A$ SD), $n=3$ (RO0281675, BAD SAHB$_A$ SD + PAA) and $n=4$ (BAD SAHB$_A$ AAA) mice. **c**, Human insulin levels in the sera of mice treated as in **a** on day 49 post transplantation. Data are from $n=6$ (Veh, BAD SAHB$_A$ SD), $n=3$ (RO0281675, BAD SAHB$_A$ SD + PAA) and $n=4$ (BAD SAHB$_A$ AAA) mice. **d**, Mean blood glucose levels during an intraperitoneal GTT and corresponding area under the curve (AUC) in mice treated as in **a** on day 42 post transplantation. The number of mice per condition is as in **c**. Data are means ± s.e.m. from independent experiments with statistical analyses using one-way ANOVA with Tukey adjustment for multiple comparisons.

link mediating this previously unappreciated connection between glucose and arginine metabolism. The ureagenic effect of PC is consistent with the notion that its activity can promote the availability of aspartate to feed the argininosuccinate shunt in support of the urea cycle. Our findings also suggest that altered urea cycle activity and an imbalance between arginine partitioning to urea versus NO synthesis is not limited to inflammation, and may be a general metabolic feature of cellular stress that can be countered by PC-directed ureagenesis (Fig. 7g).

PC is known to play an important role in anaplerotic regulation of the TCA cycle and makes a substantial contribution to aspartate synthesis in multiple cell types[25,26]. In β-cells, PC-dependent trans-mitochondrial pyruvate cycles produce metabolic signals that regulate insulin secretion[27–30]. To our knowledge, however, this is the first direct demonstration that PC regulates arginine utilization for ureagenesis while suppressing its use for NO synthesis, and that this elicits a genuine pro-survival effect. Our findings also provide mechanistic insights relevant to inborn errors of metabolism involving PC deficiency where a correlation between decreased circulating urea levels, hyperammonaemia and lower PC activity has been reported but not fully understood[31]. Furthermore, given that PC activity is altered in a number of pathologic conditions such as diabetes, cancer and certain infectious diseases[32], our findings warrant investigation into whether and how changes in ureagenesis, NO synthesis and nitrogen metabolism are linked to the disease outcomes in these settings.

Table 1 | Statistical comparisons of blood glucose levels in diabetic mice transplanted with human donor islets shown in Fig. 6

Comparison	*P* value
Vehicle vs. RO0281675	0.7507
Vehicle vs. BAD $SAHB_A$ SD	0.0014
Vehicle vs. BAD $SAHB_A$ AAA	0.5685
Vehicle vs. BAD $SAHB_A$ SD + PAA	0.9411
BAD $SAHB_A$ SD vs. RO0281675	0.0100
BAD $SAHB_A$ SD vs. BAD $SAHB_A$ AAA	0.0085
BAD $SAHB_A$ SD vs. BAD $SAHB_A$ SD + PAA	0.0114
BAD $SAHB_A$ AAA vs. RO0281675	0.9997
BAD $SAHB_A$ SD + PAA vs. BAD $SAHB_A$ AAA	0.0933
BAD $SAHB_A$ SD + PAA vs. RO0281675	0.0828

One-way ANOVA with multiple-comparisons test comparing means of each condition versus the other for every day that blood glucose was measured; Veh $n=6$, RO0281675 $n=3$, BAD $SAHB_A$ SD $n=6$, BAD $SAHB_A$ AAA $n=4$ and BAD $SAHB_A$ SD + PAA $n=3$ mice per group. *P* values were calculated using one-way ANOVA with Tukey adjustments for multiple comparisons; additional details for statistical analyses are provided in Supplementary Tables 2 and 3.

Methods

Human islets. Primary human islets freshly isolated from deceased donors were obtained from the Alberta Islet Distribution Program (University of Alberta) or provided by the Integrated Islet Distribution Program (IIDP) at City of Hope (http://iidp.coh.org/) and Prodo Labs (https://prodolabs.com/human-islets-for-research/). All donor material was obtained with informed consent and de-identified patient information, qualifying all human-islet distribution centres as IRB-exempt and thus exempt from requiring approval by the office for human research studies at Dana-Farber Cancer Institute.

A total of 109 human donors were used in this investigation with mean age of 49 ranging from 17–75 years of age, 54% and 46% of whom were males and females, respectively. The average body mass index (BMI) of donors was 26.7 (range 19.1–38.5), and baseline islet viability was 87.6% (range 68–98%). Donors obtained from IIDP are from the following Research Resource Identifiers: RRID:SAMN08769195 (University of Pennsylvania (UPenn)), RRID:SAMN08769390 (University of Wisconsin (UWisconsin)), RRID:SAMN08769393 (Sharp/Lacy), RRID:SAMN08769822 (UWisconsin), RRID:SAMN08769830 (Sharp/Lacy), RRID:SAMN08930666 (University of Illinois at Chicago), RRID:SAMN08773762 (UWisconsin), RRID:SAMN08773728 (University of Miami (UMiami)), RRID:SAMN08773856 (UMiami), RRID:SAMN08773865 (Scharp–Lacy Research Institute (Scharp/Lacy)), RRID:SAMN08769188 (Scharp/Lacy), RRID:SAMN08769207 (Southern California Islet Cell Resources Center (SC-ICRC)), RRID:SAMN08769084 (Scharp/Lacy), RRID:SAMN08769130 (UWisconsin), RRID:SAMN08769124 (SC-ICRC), RRID:SAMN08769080 (Scharp/Lacy), RRID:SAMN08769078 (UMiami), RRID:SAMN08769070 (SC-ICRC), RRID:SAMN08769066 (Scharp/Lacy), RRID:SAMN08768765 (UPenn), RRID:SAMN08768788 (UPenn), RRID:SAMN08768781 (UPenn), RRID:SAMN08611143 (UWisconsin), RRID:SAMN08616281 (Scharp/Lacy), RRID:SAMN08685106 (SC-ICRC), RRID:SAMN08848150 (SC-ICRC), RRID:SAMN09768368 (UMiami) and RRID:SAMN10079665 (UWisconsin).

Type 2 diabetic donor islets used in Fig. 1e were from two donors: a 46-yr-old female with BMI of 36 (RRID:SAMN08768788, UPenn), and a 45-year-old male with a BMI of 27 (RRID:SAMN08616281, Scharp/Lacy). Both donors had a family history of diabetes and obesity.

Islet culture and cytokine treatment. Human islets were maintained in PIM(S) medium (Prodo Labs) with 5% human A/B serum (Gemini BioProducts) at a density of 1,000 islets per 10 mL as previously described[33]. Primary mouse islets were isolated from 10-week-old C57B6 wild-type mice and cultured as previously described[12]. Control-treated mice were littermates with experimental treatments. Only male mice were used in this study. The cocktail of inflammatory cytokines (R&D Systems) used to treat human islets consisted of 10 ng mL^{-1} TNF-α, 10 ng mL^{-1} IL-1β and 100 ng mL^{-1} IFN-γ, and that used to treat mouse islets or INS-1 cells consisted of 20 ng mL^{-1} TNF-α, 40 ng mL^{-1} IL-1β and 10 ng mL^{-1} IFN-γ. These cytokine concentrations are consistent with published reports in human and mouse islets[34,35]. For AS-supplementation experiments (Fig. 4f,g and Fig. 7d, e), PIMS medium was supplemented with argininosuccinic acid disodium salt hydrate (Sigma Aldrich) at 1 mM. This concentration was selected on the basis of dose-response studies to determine AS concentrations that effectively increase urea levels in human islets (10–200 μM AS had no effect on urea levels). Of note physiological range of AS concentrations in humans is currently unknown and current methods can only detect serum levels of AS in human subjects with ASL deficiency[36]. For chronic high glucose (glucotoxic) culture conditions (Fig. 7f,h,i), islets were cultured in 33 mM glucose for 72 h compared to 5.8 mM glucose, which is the glucose concentration in PIM(S) medium used for normal culture conditions.

SAHB synthesis and treatment. Peptide synthesis, olefin metathesis, fluorescein isothiocyanate (FITC) derivatization, reverse-phase high-performance liquid chromatography (HPLC) purification and amino acid analysis were performed as previously described[12,16]. SAHBs modelled after human and mouse BAD BH3 domain variants were used for treatment of human and mouse islets, respectively. BAD $SAHB_A$ SD is modelled after phospho-mimic S118 and S155 in the human and mouse BAD sequences, respectively[12,16,18]. BAD $SAHB_A$ AAA is modelled after a triple-alanine mutant[12,19] in the BAD BH3 domain that modifies L151, S155 and D156 in the mouse BH3 domain and their corresponding residues in the human BAD BH3 sequence. The BAD AAA BH3 variant does not activate GK[12,19] (Extended Data Fig. 1c). Neither BAD $SAHB_A$ SD nor BAD $SAHB_A$ AAA binds to BCL-2/BCL-W/BCL-X_L[16]. For survival assays and human donor islet treatments, islets were treated with SAHBs for 5 h with 5 μM of the indicated SAHBs in 0.5% DMSO in uptake medium, which consisted of RPMI for mouse islets or PIM(S) for human islets, pH 6.2, which is the optimal pH for cellular uptake of BAD stapled peptides[12]. Control islets were treated with vehicle composed of 0.5% DMSO in uptake medium. Islets were then washed and left to recover in complete physiological medium (pH 7.4) prior to any further treatments or assays.

Treatment with GKAs and pharmacologic inhibitors. RO0281675 (Axon Medchem) and GKA50 (Tocris) were dissolved in DMSO and used at 5 μM in 0.5% DMSO. The following reagents were diluted in water: ABH (2(S)-amino-6-boronohexanoic acid hydrochloride, 6-borono-L-norleucine ammonium salt (Santa Cruz)) used at 50 μM, BPTES (bis-2-(5-phenylacetamido-1,3,4-thiadiazol-2-yl) ethyl sulphide, Sigma) used at 500 nM, and PAA (phenyl acetic acid, Sigma) used at 1 mM.

Quantification of NO and cell survival by flow cytometry. NO levels were measured 24 h after cytokine treatment. Briefly, 50 islets per replicate were gently dispersed in accutase (Millipore Sigma) at 37 °C, rinsed in 1 mL PBS and subsequently stained at 37 °C for 30 min with DAF-FM (Molecular Probes) for NO levels. Mean FITC signal intensities of DAF-FM stained cells were normalized to the PBS vehicle control set to 1.0 within a given experiment. Cell survival/death was quantified 48 h after cytokine treatment by staining islets with Annexin V/7AAD (BD Biosciences) as previously described[12]. Cells were monitored for PE/APC (585 nm/660 nm) or FITC/DCF (530 nm/488 nm) fluorescence using a BD FACSCanto II flow cytometer (BD Biosciences) and FACSDiva software (BD Biosciences). Positive cells were identified by comparison with unstained cells for all wavelengths at least 2 s.d. outside the means of unstained samples. See the Supplementary Methods for the gating strategies.

Genetic manipulation of islets. All infections were carried out 24 h prior to SAHB/cytokine treatment for a total of 48 h (when measuring NO levels) or 72 h (when measuring cell viability). GK Y214C mutant (pLenti-C-Myc-DDK, Origene), PC (pDNR223, Harvard Plasmid database) and ARG2 (pENTR223, Harvard Plasmid database) were first recombined into pLenti7.3 using the LR Clonase kit (Invitrogen). Lentiviruses were then packaged according to TRC Sigma protocol in 293T cells. Sigma TRC collection shRNA sequences for GK, GOT1, GOT2 and PC are as follows: human GKsh, 5′-CCGGCGAGGACGTAATGCGCATCACCTCG AGGTGATGCGCATTACGTCCTCGTTTTTTG-3′; human GOT1 sh1, 5′-CC GGGCGTTGGTACAATGGAACAAACTCGAGTTTGTTCCATTGTACCAAC GCTTTTTG-3′; GOT1 sh2, 5′-CCGGGCTAATGACAATAGCCTAAATCTCGA GATTTAGGCTATTGTCATTAGCTTTTTG-3′; human GOT2 sh1, 5′-CCGGG CCTTCACTATGGTCTGCAAACTCGAGTTTGCAGACCATAGTGAAGGCT TTTTG-3; GOT2 sh2, 5′-CCGGGCTACAAGGTTATCGGTATTACTCGAGTA ATACCGATAACCTTGTAGCTTTTTG-3′; GOT2 sh3, 5′-CCGGCGAGATGT CTTTCTGCCCAAACTCGAGTTTGGGCAGAAAGACATCTCGTTTTTG-3′; mouse PC sh1, 5′-CCGGCCCTTCAGCTATTTGTCCTTTCTCGAGAAAGGA CAAATAGCTGAAGGGTTTTG-3′; and mouse PC sh2, 5′-CCGGGCACTACT TCATCGAGGTCAACTCGAGTTGACCTCGATGAAGTAGTGCTTTTTG-3;, human PC sh1, 5′-CCGGCATGTTCATCTCTTGCCAAATCTCGAGATTT GGCAAGAGATGAACATGTTTTTG-3′; and human PC sh2, 5′-CCGGA TGGGCATCCGCCTGGATAATCTCGAGATTATCCAGGCGGATGCCCA TTTTTTTG-3′. For lentiviral expression of full-length BAD BH3 mutants (Figs. 1b and 2f and Extended Data Figs. 1a, 3c and 6c), the complementary DNAs corresponding to the BAD phosphomimic mutant (S155D) and the phospho-deficient, non-GK activating BAD AAA mutant (described above) were cloned into the pCDH vector through the services of RxBiosciences. Lentiviral-mediated knockdown and overexpression in human islets was performed as previously described[33]. For all genetic manipulations, corresponding changes in protein expression were verified by western blot analysis using the

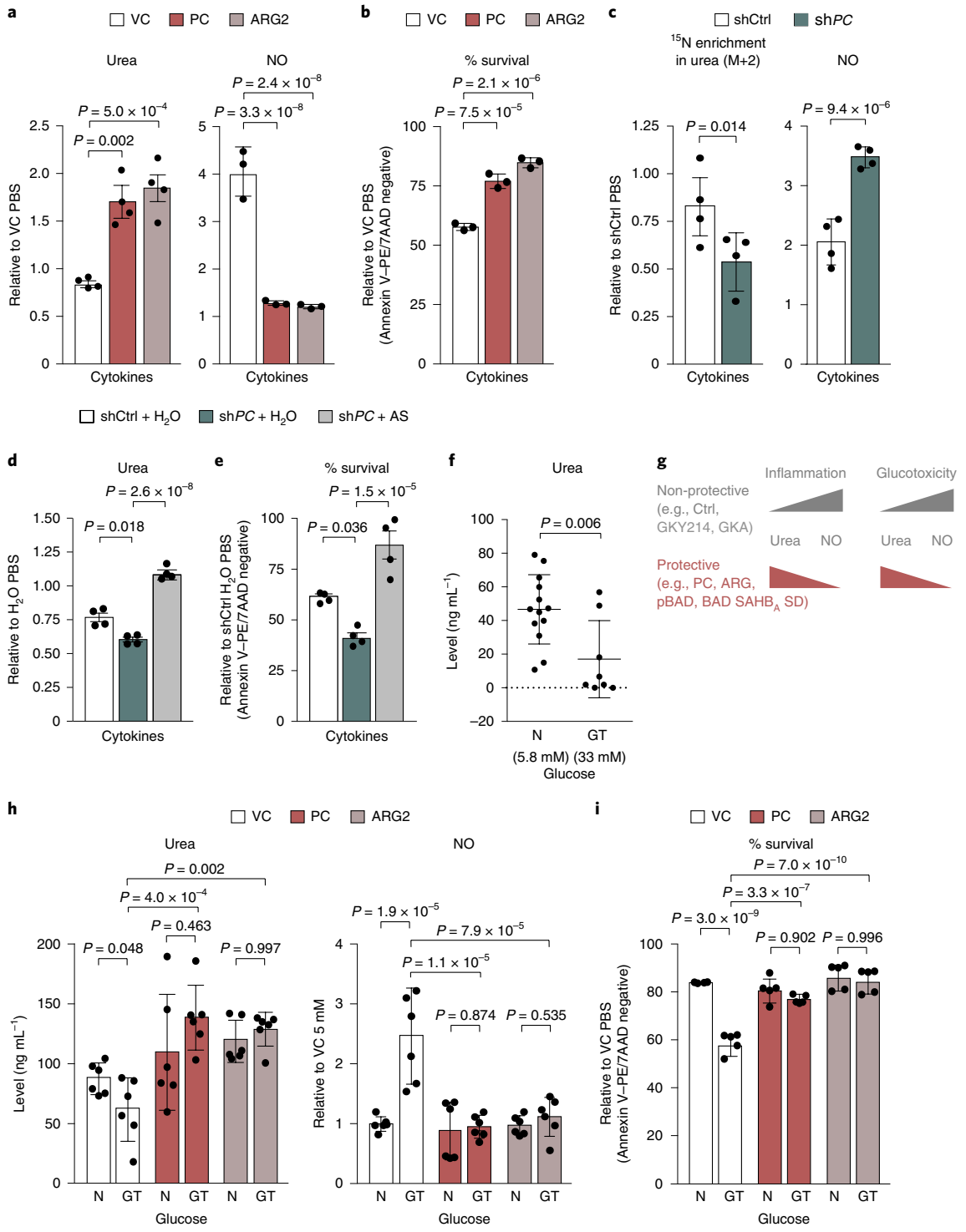

Fig. 7 | PC is sufficient to promote ureagenesis, restrict NO, and protect human islets from inflammation and glucotoxicity. a,**b**, Quantification of urea and NO levels (**a**) and viability (**b**) in human islets expressing PC or ARG2 in the presence of inflammatory cytokines; $n = 4$ human donors for urea and $n = 3$ donors for NO and viability measurements. **c**, Contribution of arginine to urea synthesis and quantification of NO levels in *PC*-depleted human islets that were labeled with [$^{15}N_2$]arginine and treated with cytokines; $n = 4$ donors. **d**,**e**, Quantification of urea levels (**d**) and viability (**e**) in human islets subjected to *PC* knockdown and exposed to cytokines in the absence (H_2O) or presence of argininosuccinate (AS). Data are means ± s.e.m of $n = 4$ independent experiments from 2 donors. **f**, Urea concentrations in human islets cultured in normal (N) medium with 5.8 mM glucose compared to glucotoxic (GT) conditions as in 72 h culture in 33 mM glucose; $n = 13$ donors for N and $n = 8$ donors for GT. Statistical analysis was performed using Student's *t*-tests. **g**, Schematic summary of results showing protective versus non-protective glucose metabolism and PC-directed urea cycle activation as a mechanism that shields cells from stress-induced augmentation in NO and cytotoxicity similar to ARG overexpression or protective GK activation. **h**,**i**, Quantification of urea and NO levels (**h**) and viability (**i**) in human islets expressing PC or ARG2 and cultured as in **f**; $n = 3$ donors in duplicates for urea and NO, and $n = 5$ donors for viability assays. Data are means ± s.e.m. from independent experiments with statistical analyses using one-way (**a**–**e**) and two-way (**h**,**i**) ANOVA with Tukey adjustment for multiple comparisons.

following antibodies and dilutions; GOT1 (Sino Biological 14196-T52-50, 1:1,000), GOT2 (My Bio Source MBS769801, 1:2,000), glucokinase (Santa Cruz, 1:1,000), pyruvate carboxylase (PCB, Santa Cruz, 1:1,000), ARG2 (Life Technologies, 1:1,000), V5 (Cell Signaling, 1:1,000), MYC-tag (Cell Signaling, 1:1,000), BAD (Abcam, 1:3,000) and actin (Sigma, 1:20,000).

Biotin–SAHB peptide pull-down assays. INS-1 cells (1×10^7) cultured in 10-cm plates were lysed on ice for 20 min in buffer containing 20 mM Tris-HCl pH 8.0, 137 mM NaCl, 2 mM $MgCl_2$, 1 mM EDTA, 0.1% CHAPS, protease and phosphatase inhibitors (Sigma Aldrich). Protein concentrations of spin-clarified lysates were determined using the BCA Protein assay kit (Thermo Fisher Scientific). Biotin pull-down assays were adapted from Escudero et al.[37]. Briefly, 200 µg of lysates were pre-incubated with 25 µM of biotinylated SAHB peptides (Extended Data Fig. 1d) or DMSO for 2 h at 4 °C. Biotinylated peptides were then captured with the addition of 30 µL of streptavidin agarose beads for 2 h at 4 °C. Beads were centrifuged at 3,000 r.p.m. for 30 s, washed and eluted by boiling in 2× LDS sample buffer (Thermo Fisher Scientific). Eluates were fractionated on SDS–polyacrylamide gel electrophoresis and subjected to western blotting with antibodies against GK and PC.

Isothermal titration calorimetry measurements. All calorimetric experiments were carried out using an Affinity isothermal titration calorimetry from TA Instruments (New Castle) equipped with autosampler in a buffer containing 20 mM HEPES pH 7.5, 150 mM NaCl and 0.5 mM TCEP, with 5% DMSO at 25 °C. Recombinant GK protein solution (40 µM) or buffer (as control) in the calorimetric cell was titrated by injecting 3 µL of 300 µM BAD BH3 $SAHB_A$ SD or the corresponding unstapled peptide solution in 200-s intervals with stirring speed at 75 r.p.m. Resulting isotherm was subtracted against buffer run and fitted with a single site model to yield thermodynamic parameters of ΔH, ΔS, stoichiometry and K_d using NanoAnalyze software (TA instruments).

Untargeted metabolomics. These analyses were performed using the services provided by General Metabolics. Human donor islets were treated as indicated above, rinsed in 150 mM ammonium formate and stored at −80 °C. Polar metabolites from 150 human islets per replicate were extracted by hot 70% ethanol at 75 °C for 3 min, vortexed, placed on ice and spin clarified. Extracts were analysed by non-targeted, flow-injection metabolomics on an Agilent 6550 Quadrupole Time-of-Flight Mass Spectrometer (Agilent) using negative ionization, as previously reported[38]. Briefly, 1.5 µL was injected using a MPS3 autosampler (Gerstel). The mobile phase consisted of isopropanol/water (60:40, vol/vol) 1 mM ammonium fluoride with a flow rate of 150 µL per min. For online mass axis correction, homotaurine and hexakis(1H,1H,3H-tetrafluoropropoxy)phosphazine (HP-0921, Agilent Technologies) were added to the mobile phase. Mass spectra were recorded in profile mode from *m/z* 50 to 1,000 with a frequency of 1.4 spectra per s for 0.48 min using the highest resolving power (4 GHz HiRes). Source temperature was set to 325 °C, with 5 L per min drying gas and a nebulizer pressure of 30 psig. Ions were putatively annotated by matching their measured mass with that of the compounds listed in KEGG database for *Homo sapiens*, allowing a tolerance of 0.001 Da, only deprotonated ions (without adducts) were included and duplicate matches were retained. Log fold change in metabolite signal intensities normalized to the median are presented for all conditions in a heat map (Extended Data Fig. 2), in which each column represents individual replicates of pooled extracts from five independent human donors, with a total of eight replicates. Data were analysed as described below under 'Metabolomics data and statistical analyses'.

Steady-state urea quantification by gas chromatography–mass spectrometry. Polar metabolites were extracted in 100 µl of 80% methanol (GC grade, Thermo Optima) added to 100 µL of spent medium from human or mouse islets (60 islets per 2 mL) and lysed by sonication. Extracts were spin-clarified, and supernatants were collected and dried by vacuum centrifugation at 4 °C (Labconco). Dried supernatant pellets were resuspended in 10 mg per mL methoxylamine in pyridine (Sigma), incubated for 30 min at 37 °C, and derivatized by silylation with 70 µL of *N*-methyl-*N*-*tert*-butyldimethylsilyltrifluoroacetamide (MTBSTFA, Sigma) for 1 h at 70 °C. After spin clarifying, 1 µL of derivatized sample was injected in splitless mode into an Agilent 5977B/7890B gas chromatography–mass spectrometry (GC–MS) with a DB-5ms capillary column with DuraGuard (Agilent Technologies), using chromatographic methods as previously described[39]. Data are shown either as concentrations (ng mL^{-1}) using a urea standard (Sigma) calibration curve or as values relative to PBS-treated controls. Between-sample differences were corrected for by a factor of median chromatographic peak area.

Arginine tracer studies. Human islets (150 in 2 mL medium) were incubated in L-[$^{15}N_2$-guanidino]arginine (Cambridge Isotopes, 200 mg per L) for 72 h in RPMI medium containing 5.5 mM glucose with 5% human A/B serum. At this time point, endogenous arginine pools were saturated with the label. Cytokine treatment was performed 24 h prior to collection. For quantification of M+*n* urea, medium was collected (200 µL per replicate) and polar metabolites were extracted in 800 µL of 100% methanol, spin-clarified and dried by vacuum centrifugation at 4 °C (Labconco). Derivatization, instrumentation and data collection was the same as described above for steady-state urea measurement using GC–MS. The 1–1,000 ng [$^{15}N_2$]urea (Cambridge Isotopes) standard was assayed in the same medium in parallel to generate a concentration curve for direct quantification of [$^{15}N_2$]urea in experimental samples (retention time 13.6 min, target ions 213/215 and qualifier ions 233/235 for M+0/M+2 urea). Mass isotopomer distributions (MIDs) were calculated from proportional ion counts with corrections for natural abundances, individual chromatogram data were normalized to tracer uptake and subsequently compared with the amount in vehicle PBS-treated control set to 1.0. For quantification of M+*n* arginine and citrulline, islets were washed with cold 150 mM ammonium formate solution pH of 7.4 and extracted with 600 µL of 31.6% methanol/36.3% ACN in H_2O (vol/vol). Cells were lysed and homogenized by bead-beating for 2 min at 30 Hz using 6.2-mm ceramic beads per sample (TissueLyser II, Qiagen). Cellular extracts were partitioned into aqueous and organic layers following dimethyl chloride treatment and centrifugation. The aqueous supernatants were dried as above, subsequently resuspended in 30 µL of chilled H_2O and clarified by centrifugation at 1 °C. Each sample was analysed three times using 5 µL injections in an Agilent 6540 UHD Accurate-Mass Q-TOF Mass Spectrometer (Agilent Technologies) equipped with a 1290 Infinity Ultra-Performance LC System (Agilent Technologies). Analyte ionization was accomplished using electrospray ionization in positive mode. The source operating conditions were set at 325 °C and 9 L per min for gas temperature and flow, respectively, nebulizer pressure was set at 40 psi and capillary voltage was set a 4.0 kV. Reference masses 121.0509 and 922.0099 were introduced into the source through a secondary spray nozzle to ensure accurate mass. MS data were acquired in full-scan mode, mass range: *m/z* 100–1000, scan time: 1.4 s, data collection: centroid and profile modes. Retention times, accurate masses and MS/MS (10, 20, 30, 40 V) for each compound were confirmed against authentic standards; [$^{15}N_2$]arginine and [$^{15}N_1$]citrulline (Cambridge Isotopes). Unlabelled islet extracts and quality-control NT2196 cell extracts were used to confirm that signals were free of interfering ions in the mass range of interest. Chromatographic separation was performed using an Intrada Amino Acid column 3 µm, 3.0×150 mm (Imtakt Corp). The chromatographic gradient started at 100% mobile phase B (0.3% formic acid in ACN) with a 3-min gradient to 27% mobile phase A (100 mM ammonium formate in 20% ACN/80% water) followed with a 19.5-min gradient to 100% A at a flow rate of 0.6 mL min^{-1}. This was followed by a 5.5-min hold time at 100% mobile phase A and a subsequent re-equilibration time (7 min) before the next injection. The column temperature was maintained at 10 °C. Retention times for arginine and citrulline were 19.6 min and 8.5 min, respectively. Data are reported as ^{15}N enrichment, which is the corrected ^{15}N isotopomer abundance normalized to the total abundance of a given metabolite, which was also normalized to tracer uptake and subsequently compared with the amount in vehicle PBS-treated control set to 1.0.

Glucose tracer studies. Mouse islets were incubated with 11 mM of uniformly labelled [$^{13}C_6$]glucose (Cambridge Isotopes) in RPM1640 (Sigma Aldrich) for 24 h with simultaneous PBS or cytokine treatment. Polar metabolites from 150 islets were extracted in 80% methanol, derivatized and detected with the same methods as above for steady-state urea measurement using GC–MS. MID analysis was performed using a previously described algorithm[40] and is described below under metabolomics data analysis. Data are reported as ^{13}C isotopomer enrichment compared to the total abundance of a given metabolite and normalized to vehicle PBS-treated control set to 1.0 (Figs. 4c and 5a, and Extended Data Fig. 6a,b) and as ^{13}C fractional labelling not normalized to vehicle PBS in Extended Data Fig. 5a.

Metabolomics data and corresponding statistical analysis. All data except the untargeted metabolomics analysis were quantified by integrating the area under the curve of each metabolite and its isotopologue using MassHunter Quant (Agilent Technologies). Each metabolite's accurate mass ion and subsequent isotopic ions were extracted (EIC) using a 10 ppm window. In the case of isotopic labelling with [$^{13}C_6$]glucose or [$^{15}N_2$]arginine, corrections for natural enrichments were generated for each metabolite (C_{total}^{-1} or N_{total}^{-1}) using a previously developed algorithm[41]. MIDs of the indicated metabolites were calculated as previously described[41] and expressed as percentage of the untreated PBS control set at 1.0. Pathway enrichment, PCA, fold change and ANOVA statistical analyses were performed using Metaboanalyst software (www.metaboanalyst.ca). Pathway analysis was performed to compare the $\log_2$(fold change) data between two conditions per analysis, BAD $SAHB_A$ SD versus vehicle, and BAD $SAHB_A$ SD versus RO0281675, all in the presence of cytokines (Fig. 1i).

PC enzymatic assay. PC activity was measured in 150 human lysed by sonication in 100 µL MOPS lysis buffer with protease inhibitors cocktail (Roche) and incubated with $NaH^{14}CO_3$, as previously described[42]. Briefly, 25 µL of lysate per reaction replicate or control lysate without substrate (pyruvate) containing $NaH^{14}CO_3$, were maintained at 37 °C for 60 min and stopped with 10% TCA, according to previously described methods[42]. Reactions were loaded onto P81 filter paper and volatile non-incorporated $NaH^{14}CO_3$ was removed and $^{14}CO_2$ incorporation was measured by liquid scintillation. PC activity is reported as nmol $^{14}CO_2$ calculated from total ^{14}C counts after subtracting ^{14}C in control samples without pyruvate, normalized to protein content.

FACS purification of human β-cells for proteomic and RNA-seq analyses. Human islets obtained from Prodo Labs were dispersed using Accutase (MT25058CI, Thermo Fisher Scientific) and infected with an adenovirus expressing the bright green fluorescent protein, ZsGreen (Clontech) under control of the rat insulin-1 promoter (RIP1) and a mini-CMV enhancer. The RIP1-mini-CMV promoter included 177 bases of the hCMV IE-1 promoter ClaI-SpeI fragment ligated to 438 bases of the RIP1 promoter[43,44]. Following transduction with the Ad.RIP-ZsGreen adenovirus for 2 h, RPMI1640 medium containing 10% FBS was added to terminate adenovirus infection. Cells were collected 96 h after infection and loaded onto an Aria II Cell Sorter (BD biosciences), and the live ZsGreen$^+$ cell (β-cells) FITC-positive population was collected. The β-cell fraction was confirmed to be >92% pure by immunolabelling of sorted cells with insulin, and independently, by qRT–PCR and by RNA-seq[43,44]. This procedure was repeated several times using islets from $n=3$ donors, and sorted β-cells were pelleted and frozen at −80 °C until enough starting materials for proteomic analyses were obtained. The donors were non-diabetic, with BMIs of 26.3, 28.8 and 27 and ages 48, 61 and 63, respectively. Please see the Supplementary Methods for the gating strategy.

Multidimensional nanoflow LC–MS/MS proteomic analysis of FACS-purified human β-cells. Lysis buffer (1% SDS, 50 mM HEPES, with protease and phosphatase inhibitors) was added to frozen β-cell pellets (purified and collected as above), and the mixture was heated to 95 °C for 5 min. After treatment with 25 U benzonase (Novagen, Thermo Fisher Scientific) for 30 min at 37 °C, proteins were reduced with 10 mM DTT for 30 min at 56 °C, alkylated with 22.5 mM iodoacetamide for 30 min in the dark and captured on magnetic beads as described[45]. After 3 washes (2 × 70% ethanol and 1 × 100% ethanol), beads were reconstituted with 100 mM ammonium bicarbonate and proteins digested overnight with trypsin at 37 °C. Peptides were re-captured on the magnetic beads by adding acetonitrile to a final concentration of 95%[45]. After washing with acetonitrile, peptides were eluted in 2% DMSO with 50 mM ammonium formate, pH 10, and analysed by DEEP-SEQ mass spectrometry[46] at a depth of 34 fractions using a NanoAcquity UPLC system (Waters) coupled to a timsTOF Pro ion mobility mass spectrometer (Bruker). Peptide fractions were eluted from the first dimension, reversed phase column (5 cm × 150 µm packed with 5 µm XBridge C18, Waters) and second dimension anion exchange column (5 cm ×150 µm I.D. fused silica packed with 10 µm POROS 10HQ, Applied Biosystems) using injections of acetonitrile or ammonium formate at pH 10.0. Peptide fractions were diluted in-line with solvent A (0.2 M acetic acid in water) to reduce pH and organic concentration and facilitate retention on the final dimension precolumn (5 cm × 100 µm I.D. fused silica packed with 7 µm Symmetry C18, Waters). Peptides were eluted with an HPLC gradient (5–35% B in 120 minutes, A = 0.2 M acetic acid in water, B = 0.2 M acetic acid in acetonitrile), resolved on an analytical column (30 µm I.D. × 50 cm Monitor C18, Orochem), and introduced to the mass spectrometer by electrospray ionization using a captive spray ion source (spray voltage = 1.6 kV). The mass spectrometer collected ion mobility MS spectra over a mass range of m/z 100–1,700 and 1/k0 of 0.6 to 1.6, and then performed 10 cycles of PASEF MS/MS with a target intensity of 20k and a threshold of 250. Active exclusion was enabled with a release time of 0.4 min. MS/MS spectra were matched to peptide sequences from human proteins in the UniProt database (downloaded 4 September 2018) using PEAKS Studio 10.0 software[47]. Search parameters specified precursor and production tolerances of 20 ppm and 50 mmu, respectively, as well as fixed carbamidomethylation and variable oxidation of methionine. Search results were filtered to a false-discovery rate of 1% and exported to csv. After mapping peptide sequences to unique gene identifiers using the Pep2gene tool[48], multiplierz scripts[49] were used to provide an estimate of relative protein expression[50] based on the three most abundant peptides detected for each gene product. Data in Fig. 3a are the distribution of the relative abundance levels of all proteins detected except those that had less than 3 unique peptides identified. The complete raw dataset with accession numbers and signal intensities can be found in online Supplementary Table 1. Native mass spectrometry data files are available for download from the MassIVE archive at the University of California, San Diego (ftp://massive.ucsd.edu/MSV000085082/).

RNA-seq expression analysis of FACS-purified human β-cells. The RNA-seq data in Fig. 3b are taken from a previously published dataset from non-diabetic donors[43]. Briefly, RNA was prepared from freshly FACS-purified human β-cell using the RNeasy Micro kit (Qiagen). RNA yields were 300–500 ng from each FACS purification, and RNA integrity numbers were between 9.5 and 10.0. PolyA$^+$ messenger RNA from sorted β-cells was purified with oligonucleotide dT magnetic beads. The polyA$^+$ RNA from β-cells was then fragmented in the presence of divalent cations at 94 °C. The fragmented RNA was converted into double-stranded cDNA. After polishing the ends of the cDNA, the 3′ ends were adenylated. Lastly, Illumina-supplied universal adapters were ligated to the cDNA fragments. The adapter-ligated DNA was size selected to get an average of 250-bp insert size using AmpPure beads and amplified by 15-cycle PCR. The PCR DNA was then purified using AmpPure beads to get the final seq library ready for sequencing. The insert size and DNA concentration of the seq library was determined on Bioanalyzer (Agilent Technologies) and Qubit (Thermo Fisher Scientific), respectively. A pool of 10 barcoded RNA-seq libraries was layered on 2 of the 8 lanes of the Illumina flow cell at appropriate concentration and bridge amplified to yield ~25–35 million raw clusters. The DNA reads on the flow cell were then sequenced on HiSeq 2000 using a 100-bp paired-end recipe. Results are expressed as $\log_2$-transformed signals for millions of counts (reads) per million bases ($\log_2$(CPM), Fig. 3b), and were calculated as previously described[43]. RNA enrichments in Extended Data Fig. 4 were calculated using a transcriptome dataset for sorted β-cells, whole islet and negative-sorted islet cells generously provided by E. Dermitzakis (accession EGAS00001000442; http://www.ebi.ac.uk/ega/)[51] and corresponding reads per kilobase per million mapped reads (RPKM) values were analysed following the methodology described in Wang et al.[43]. RNA enrichments were calculated by dividing individual RPKM values for each gene from sorted β-cells and non-sorted islet cells by the whole islet RPKM values, where whole islet values are set to 1.

Immunostaining of human islets to assess expression of urea cycle enzymes in β-cells. Human islets from 3 donors were dispersed into single cells on 12-mm-diameter round coverslips (Electron Microscopy Sciences) coated with poly-D-lysine (Sigma) and cultured overnight in 48-well plates. Cells were then fixed in 3.7% formaldehyde solution (Sigma) in medium containing 1 µg per mL Hoechst (BD Pharmogen) at 37 °C for 15 min, rinsed in PBS containing 75 mg/ml glycine, treated with 0.1% Triton-X-100 for antigen retrieval, and blocked in 10% FBS (Gibco) for 1 h. Immunostaining was performed overnight at 4 °C for each of the following antibodies individually at 1:200 dilution: ARG2 (ABClonal), ASL (Sigma), ASS1 (Thermo Fisher Scientific), CPS1 (ABClonal), NAGS (ABClonal), DDAH1 (Sino Biological) and DDAH2 (ABClonal). Coverslips were rinsed three times in PBS and stained with secondary antibodies against rabbit and/or mouse conjugated to Alexa Fluor 488 (Life Technologies) at 1:500 dilution. Samples without primary antibody were used as negative controls to account for background fluorescence of secondary Alexa Fluor 488 antibodies. All coverslips were then co-stained with an antibody to insulin (LSBio) at 1:150 dilution for 1 h at room temperature, rinsed and stained with a secondary guinea-pig antibody to Alexa Fluor 568 (Thermo Fisher Scientific) at 1:500 dilution, and mounted onto microglass with ProLong Diamond Antifade mountant (Thermo Fisher Scientific). Imaging was performed on a Nikon Ti with Perfect Focus and Spinning Disk Confocal, with 488-, 445- and 561-nm lasers, a Hamamatsu ORCA-R2 cooled CCD camera and MetaMorph image-acquisition software with ×60 and ×100 objective oil-lens. Quantification was performed on 5 images per antibody with 3–5 cells per image in Fiji software (https://imagej.net) by generating a threshold selection mask in the 561 nm channel image to create an insulin-positive region of interest, which was then mapped onto the corresponding 488 image within which the intensity of the 488 nm signal was measured.

Marginal human islet mass xenotransplantation. Human islets from 14 donors were treated overnight with vehicle (1% DMSO), 5 µM of the indicated BAD $SAHB_A$ or RO0281675, or were co-treated with 5 µM BAD $SAHB_A$ SD and 1 mM PAA in 1% DMSO in RPMI SAHB uptake medium containing 11 mM glucose, 10% serum and 0.1% Tween 80 (pH 6.0) at 37 °C. Islets were then washed and incubated in fresh medium for 24 h before transplantation. The presence of $SAHB_A$ was verified up to 4 d post uptake in human islets. Donors ranged in age from 21 to 64 years (mean, 44); 6 were female and 8 were male. Mean BMI was 25 (range 20.8–32.9) and islet purity ranged from 85% to 90%. Diabetes was induced by single intraperitoneal (i.p.) injection of STZ (S0130, Sigma) at 200 mg per kg (body weight) in 200 µL total volume in a total of 22 10- to 12-week-old male NOD-SCID mice (001303, Jackson Labs), with $n=3$–6 mice per condition. STZ-treated mice were subjected to transplantation surgery 24–48 h after their blood glucose levels reached ≥300 mg dL^{-1}. Mice were anaesthetized, and a small incision was made in the skin overlying the kidney to expose the peritoneum. The kidney was then exposed by a small incision in the peritoneum and kept moist throughout the procedure. Using a 23-g needle, a small nick was made in the kidney capsule and 500 human islets pre-treated as indicated above were glided through the nick using PE50 tubing. The tubing was removed gently, and the nick cauterized. The area was then sutured, and skin staples applied. Transplant recipients were monitored daily. Blood glucose, insulin measurements and intraperitoneal GTT were performed as previously described[12]. All animal studies were performed in compliance with, and with approval of, the Icahn School of Medicine at Mount Sinai Institutional Animal Care and Use Committee.

Quantification of β-cell death in islet grafts. Kidneys were excised from transplanted mice, fixed in Bouin's solution, paraffin-embedded, sectioned and stained with an antibody to insulin (A0564, DAKO), TUNEL (G3250 DeadEnd Fluorometric TUNEL system, Promega) and DAPI (D21490, Invitrogen). Cells doubly positive for insulin and TUNEL staining were quantified and compared with the total number of insulin-positive cells using fluorescence microscopy. An average of 1,166 ± 163 cells were counted per condition and are pooled means of a total of 32 individual mouse grafts with Veh $n=6$, RO0281675 $n=5$, BAD $SAHB_A$ SD $n=6$, BAD $SAHB_A$ SD + PAA $n=4$ and BAD $SAHB_A$ AAA $n=4$ mice and reported as percentage β-cell death representing the percentage TUNEL-positive cells normalized to vehicle set to 100%. Imaging was performed at ×20

magnification with a CARL ZEISS AXIO Observer Z1 Inverted Microscope using ZEN 2 core imaging Software for Zeiss microscope.

Statistical analyses. One or two-way ANOVA with Tukey's test for multiple means comparisons and Student's *t*-test were used in GraphPad for calculating statistical significance with *q*-value adjustments for a false-discovery rate (FDR) of 1%. Outliers were rarely removed and were determined using two-sided Grubbs with α set to 0.05. In the case that an outlier was observed, the data were further inspected with the ROUT method at FDR set to 1% to check for multiple outliers.

Reporting Summary. Further information on research design is available in the Nature Research Reporting Summary linked to this article.

Data availability

The immunofluorescence data to support the conclusions of this study are available under https://doi.org/10.6084/m9.figshare.11956506 at https://figshare.com/. Uncropped western blots for Extended Data Figs. 1 and 5–7 are presented as source data with the paper. Proteomic data in Fig. 3a are available in Supplementary Table 1, and native mass spectrometry data files are available for download from the MassIVE archive at the University of California, San Diego (ftp://massive.ucsd.edu/MSV000085082/). RNA-seq data in Fig. 3b are available in https://doi.org/10.1038/s41467-017-00992-9. RNA-seq data in Extended Data Fig. 4 were obtained with permission from E. Dermitzakis (accession no. EGAS00001000442; http://www.ebi.ac.uk/ega/)[51].

Received: 31 January 2020; Accepted: 26 March 2020;
Published online: 11 May 2020

References

1. Dadon, D. et al. Glucose metabolism: key endogenous regulator of beta-cell replication and survival. *Diabetes Obes. Metab.* **14**, 101–108 (2012).
2. De Nigris, V. et al. Short-term high glucose exposure impairs insulin signaling in endothelial cells. *Cardiovasc. Diabetol.* **14**, 114 (2015).
3. Hu, C. M. et al. High glucose triggers nucleotide imbalance through o-glcnacylation of key enzymes and induces kras mutation in pancreatic cells. *Cell Metab.* **29**, 1334–1349 e1310 (2019).
4. Manzo, E. et al. Glycolysis upregulation is neuroprotective as a compensatory mechanism in ALS. *eLife* **8**, e45114 (2019).
5. Atkinson, M. A. et al. How does type 1 diabetes develop?: the notion of homicide or beta-cell suicide revisited. *Diabetes* **60**, 1370–1379 (2011).
6. Donath, M. Y., Dalmas, E., Sauter, N. S. & Boni-Schnetzler, M. Inflammation in obesity and diabetes: islet dysfunction and therapeutic opportunity. *Cell Metab.* **17**, 860–872 (2013).
7. Eizirik, D. L., Colli, M. L. & Ortis, F. The role of inflammation in insulitis and beta-cell loss in type 1 diabetes. *Nat. Rev. Endocrinol.* **5**, 219–226 (2009).
8. Kolb, H. & von Herrath, M. Immunotherapy for type 1 diabetes: why do current protocols not halt the underlying disease process? *Cell Metab.* **25**, 233–241 (2017).
9. Lee, Y. S., Wollam, J. & Olefsky, J. M. An integrated view of immunometabolism. *Cell* **172**, 22–40 (2018).
10. Mathis, D. Immunological goings-on in visceral adipose tissue. *Cell Metab.* **17**, 851–859 (2013).
11. Matschinsky, F. M. Assessing the potential of glucokinase activators in diabetes therapy. *Nat. Rev. Drug Discov.* **8**, 399–416 (2009).
12. Ljubicic, S. et al. Phospho-BAD BH3 mimicry protects beta cells and restores functional beta cell mass in diabetes. *Cell Rep.* **10**, 497–504 (2015).
13. Cuesta-Munoz, A. L. et al. Severe persistent hyperinsulinemic hypoglycemia due to a de novo glucokinase mutation. *Diabetes* **53**, 2164–2168 (2004).
14. Grimsby, J. et al. Allosteric activators of glucokinase: potential role in diabetes therapy. *Science* **301**, 370–373 (2003).
15. Cullen, K. S., Matschinsky, F. M., Agius, L. & Arden, C. Susceptibility of glucokinase-MODY mutants to inactivation by oxidative stress in pancreatic beta-cells. *Diabetes* **60**, 3175–3185 (2011).
16. Danial, N. N. et al. Dual role of proapoptotic BAD in insulin secretion and beta cell survival. *Nat. Med.* **14**, 144–153 (2008).
17. Gimenez-Cassina, A. & Danial, N. N. Regulation of mitochondrial nutrient and energy metabolism by BCL-2 family proteins. *Trends Endocrinol. Metab.* **26**, 165–175 (2015).
18. Szlyk, B. et al. A phospho-BAD BH3 helix activates glucokinase by a mechanism distinct from that of allosteric activators. *Nat. Struct. Mol. Biol.* **21**, 36–42 (2014).
19. Gimenez-Cassina, A. et al. Regulation of hepatic energy metabolism and gluconeogenesis by BAD. *Cell Metab.* **19**, 272–284 (2014).
20. McKerrecher, D. et al. Design of a potent, soluble glucokinase activator with excellent in vivo efficacy. *Bioorg. Med. Chem. Lett.* **16**, 2705–2709 (2006).
21. Koppe, L. et al. Urea impairs beta cell glycolysis and insulin secretion in chronic kidney disease. *J. Clin. Invest.* **126**, 3598–3612 (2016).
22. Stickings, P., Mistry, S. K., Boucher, J. L., Morris, S. M. & Cunningham, J. M. Arginase expression and modulation of IL-1β-induced nitric oxide generation in rat and human islets of langerhans. *Nitric Oxide* **7**, 289–296 (2002).
23. Yoshimatsu, G. et al. Pancreatic beta-cell-derived IP-10/CXCL10 isletokine mediates early loss of graft function in islet cell transplantation. *Diabetes* **66**, 2857–2867 (2017).
24. Bensellam, M., Laybutt, D. R. & Jonas, J. C. The molecular mechanisms of pancreatic beta-cell glucotoxicity: recent findings and future research directions. *Mol. Cell Endocrinol.* **364**, 1–27 (2012).
25. Cappel, D. A. et al. Pyruvate-carboxylase-mediated anaplerosis promotes antioxidant capacity by sustaining tca cycle and redox metabolism in liver. *Cell Metab.* **29**, 1291–1305 e1298 (2019).
26. Cardaci, S. et al. Pyruvate carboxylation enables growth of SDH-deficient cells by supporting aspartate biosynthesis. *Nat. Cell Biol.* **17**, 1317–1326 (2015).
27. Jensen, M. V. et al. Metabolic cycling in control of glucose-stimulated insulin secretion. *Am. J. Physiol. Endocrinol. Metab.* **295**, E1287–E1297 (2008).
28. Jitrapakdee, S., Wutthisathapornchai, A., Wallace, J. C. & MacDonald, M. J. Regulation of insulin secretion: role of mitochondrial signalling. *Diabetologia* **53**, 1019–1032 (2010).
29. MacDonald, P. E., Joseph, J. W. & Rorsman, P. Glucose-sensing mechanisms in pancreatic beta-cells. *Philos. Trans. R Soc. Lond. B Biol. Sci.* **360**, 2211–2225 (2005).
30. Prentki, M., Matschinsky, F. M. & Madiraju, S. R. Metabolic signaling in fuel-induced insulin secretion. *Cell Metab.* **18**, 162–185 (2013).
31. Garcia-Cazorla, A. et al. Pyruvate carboxylase deficiency: metabolic characteristics and new neurological aspects. *Ann. Neurol.* **59**, 121–127 (2006).
32. Lao-On, U., Attwood, P. V. & Jitrapakdee, S. Roles of pyruvate carboxylase in human diseases: from diabetes to cancers and infection. *J. Mol. Med. (Berl)* **96**, 237–247 (2018).
33. Robitaille, K. et al. High-throughput functional genomics identifies regulators of primary human beta cell proliferation. *J. Biol. Chem.* **291**, 4614–4625 (2016).
34. Nordmann, T. M. et al. The role of inflammation in beta-cell dedifferentiation. *Sci. Rep.* **7**, 6285 (2017).
35. Yang, Z. et al. Inflammatory blockade improves human pancreatic islet function and viability. *Am. J. Transplant* **5**, 475–483 (2005).
36. Ficicioglu, C., Mandell, R. & Shih, V. E. Argininosuccinate lyase deficiency: longterm outcome of 13 patients detected by newborn screening. *Mol. Genet. Metab.* **98**, 273–277 (2009).
37. Escudero, S. et al. Dynamic regulation of long-chain fatty acid oxidation by a noncanonical Interaction between the MCL-1 BH3 helix and VLCAD. *Mol. Cell* **69**, 729–743 e727 (2018).
38. Fuhrer, T., Heer, D., Begemann, B. & Zamboni, N. High-throughput, accurate mass metabolome profiling of cellular extracts by flow injection-time-of-flight mass spectrometry. *Anal. Chem.* **83**, 7074–7080 (2011).
39. Gravel, S. P., Andrzejewski, S., Avizonis, D. & St-Pierre, J. Stable isotope tracer analysis in isolated mitochondria from mammalian systems. *Metabolites* **4**, 166–183 (2014).
40. Nanchen, A., Fuhrer, T. & Sauer, U. Determination of metabolic flux ratios from 13C-experiments and gas chromatography-mass spectrometry data: protocol and principles. *Methods Mol. Biol.* **358**, 177–197 (2007).
41. McGuirk, S. et al. PGC-1α supports glutamine metabolism in breast cancer. *Cancer Metab.* **1**, 22 (2013).
42. Kerr, D., Grahame, G. & Nakouzi, G. Assays of pyruvate dehydrogenase complex and pyruvate carboxylase activity. *Methods Mol. Biol.* **837**, 93–119 (2012).
43. Wang, H. et al. Insights into beta cell regeneration for diabetes via integration of molecular landscapes in human insulinomas. *Nat. Commun.* **8**, 767 (2017).
44. Wang, P. et al. Combined Inhibition of DYRK1A, SMAD, and trithorax pathways synergizes to induce robust replication in adult human beta cells. *Cell Metab.* **29**, 638–652 e635 (2019).
45. Hughes, C. S. et al. Ultrasensitive proteome analysis using paramagnetic bead technology. *Mol. Syst. Biol.* **10**, 757–757 (2014).
46. Zhou, F. et al. Genome-scale proteome quantification by DEEP SEQ mass spectrometry. *Nat. Commun.* **4**, 2171 (2013).
47. Ma, B. et al. PEAKS: powerful software for peptidede novo sequencing by tandem mass spectrometry. *Rapid Commun. Mass Spectrom.* **17**, 2337–2342 (2003).
48. Askenazi, M., Marto, J. A. & Linial, M. The complete peptide dictionary — a meta-proteomics resource. *Proteomics* **10**, 4306–4310 (2010)..
49. Alexander, W. M., Ficarro, S. B., Adelmant, G. & Marto, J. A. multiplierz v2.0: a Python-based ecosystem for shared access and analysis of native mass spectrometry data. *Proteomics* **17**, 1700091 (2017).
50. Silva, J. C., Gorenstein, M. V., Li, G.-Z., Vissers, J. P. C. & Geromanos, S. J. Absolute quantification of proteins by LCMSE. *Mol. Cell Proteom.* **5**, 144–156 (2006).

51. Nica, A. C. et al. Cell-type, allelic, and genetic signatures in the human pancreatic beta cell transcriptome. *Genome Res.* **23**, 1554–1562 (2013).

Acknowledgements

We thank G. Yellen, B. Spiegelman, N. Kalaany and members of the Danial laboratory for helpful discussions and the Nikon Imaging Center at Harvard Medical School for access to imaging platforms. RNA expression data for comparing enrichment of genes in purified human β-cells compared to whole islets and non-β-cells (Extended Data Fig. 4) were generously provided by E. Dermitzakis. This work was supported by the US NIH grants R01DK078081 (N.N.D.), R01CA219850 (N.N.D. and J.A.M.), R01DK113079 (A.G.-O.), R01DK105015 and R01DK116873 (A.F.S.), P30DK020541 (Einstein-Sinai Diabetes Research Center) (A.G.-O. and A.F.S.), R35CA197583 (L.D.W.), R50CA211399 (G.H.B.), R01CA222218 (J.A.M.), Juvenile Diabetes Research Foundation Grant 2-SRA-2015-58-Q-R (N.N.D.) and Barry and Mimi Sternlicht Type 1 Diabetes Research Fund (N.N.D.). A.F. was supported by a postdoctoral fellowship from the Juvenile Diabetes Research foundation (JDRF). The Integrated Islet Distribution Program (IIDP) is supported by NIH Grant 2UC4DK098085. The Rosalind and Morris Goodman Cancer Research Centre Metabolomics Core Facility is supported by the Canada Foundation for Innovation, Dr. John R. and Clara M. Fraser Memorial Trust, the Terry Fox Foundation in partnership with the Foundation du Cancer du Sein du Quebec and McGill University. The Blais Proteomics Center is supported by the Dana-Farber Strategic Research Initiative. A.M.J.S. is a Fellow of the Royal Society of Canada, and is supported through a Canada Research Chair in Regenerative Medicine and Transplantation Surgery.

Author contributions

A.F. and N.N.D. designed experiments, performed and analysed metabolomics, biochemical and cell-based studies. T.K. and A.M.J.S. provided human donor islets. D.A., M.G.B., G.B., J.J.K. and R.G.J. provided expertise in metabolomics. A.G.-O. and A.F.S. provided expertise in β-cell biology. J.C.A.-P., C.R. and A.G.-O. carried out human islet xenotransplantation studies, and together with E.K. purified human β-cells. E.K. and A.F.S. performed RNA-seq analysis on purified human β-cells. S.B.F. and J.A.M. carried out proteomic analysis on purified human β-cells. G.H.B. and L.D.W. designed and synthesized stapled peptides. H-S.S. and S.D. performed isothermal titration calorimetry analyses. D.W.C. performed peptide pull-down studies. L.E. provided technical support for mouse islet isolation and in vitro studies. A.F. and N.N.D. wrote the manuscript, which was reviewed by all authors.

Competing interests

J.A.M. serves on the SAB of 908 Devices, and has received sponsored research support from AstraZeneca and Vertex. L.D.W. is a scientific co-founder and shareholder in Aileron Therapeutics. R.G.J. is a scientific advisory board member for Immunomet Therapeutics and consultant for Agios Pharmaceuticals. All other authors declare no competing interests.

Additional information

Extended data is available for this paper at https://doi.org/10.1038/s42255-020-0199-4.

Supplementary information is available for this paper at https://doi.org/10.1038/s42255-020-0199-4.

Correspondence and requests for materials should be addressed to N.N.D.

Peer review information Primary Handling Editor: Elena Bellafante.

Reprints and permissions information is available at www.nature.com/reprints.

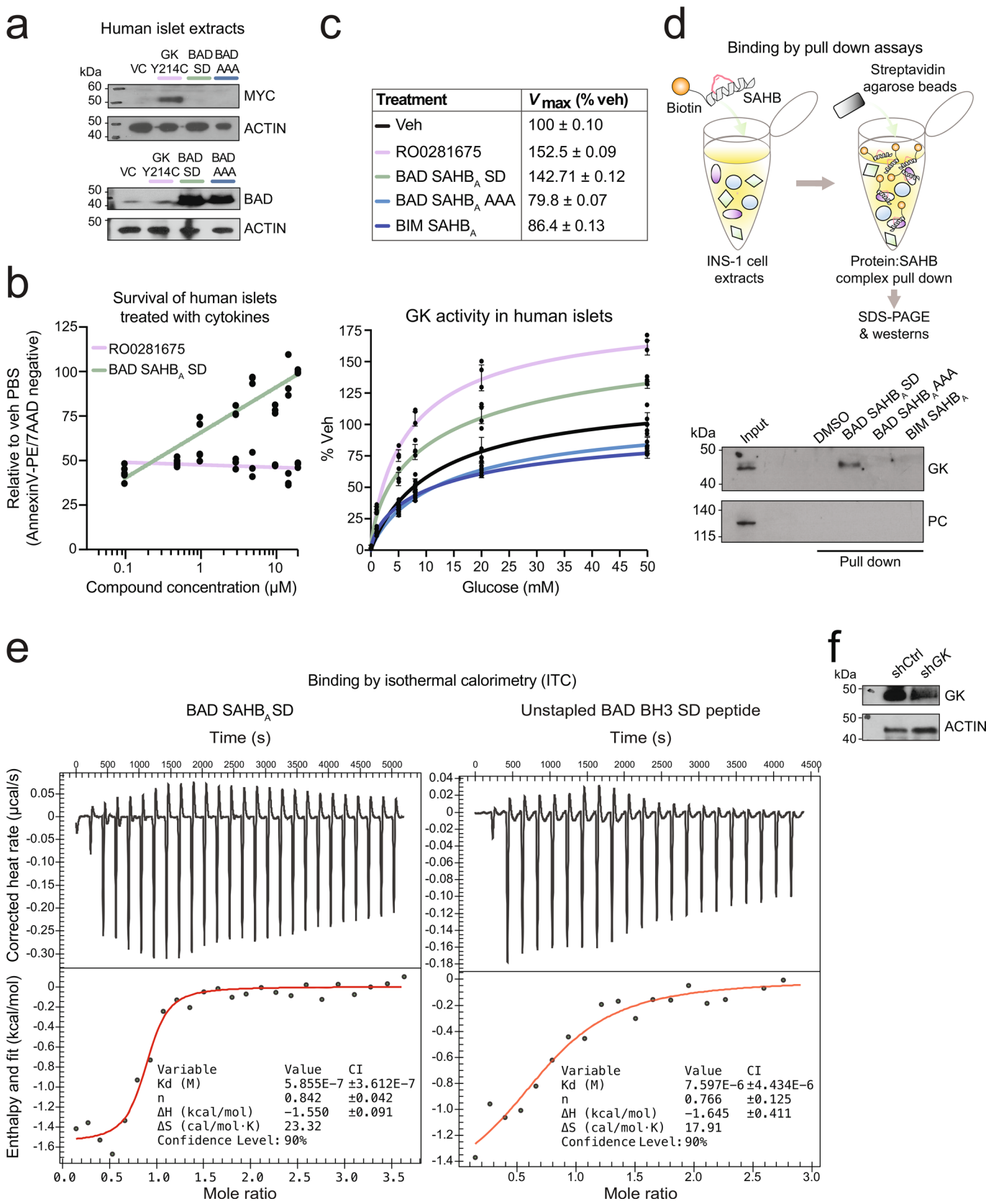

Extended Data Fig. 1 | See next page for caption.

Extended Data Fig. 1 | Characterization of GK-modulating tools used in this study. a, Western blots showing expression levels of full length MYC-tagged GK Y214C and BAD BH3 mutant proteins in islets used in Figs. 1b and 2f. Blots are representative of n = 2 independent experiments with similar results. **b**, Viability of human islets treated with increasing doses of RO0281675 or BAD $SAHB_A$ SD and exposed to cytokines as in Fig. 1c. Based on these dose response studies, we elected to use RO0281675 at 3 μM and BAD $SAHB_A$ SD at 5 μM throughout all studies. Data are means ± s.d. of 3 technical replicates of islet cultures from one human donor. **c**, GK activity in human islets treated with vehicle (DMSO), RO0281675, BAD $SAHB_A$ SD, BAD $SAHB_A$ AAA or a stapled peptide modeled after the BH3 domain of a related BCL-2 family protein (BIM $SAHB_A$). Data are means ± s.d. with n = 4 (Veh and BAD $SAHB_A$ SD) or n = 3 (RO0281675, BAD $SAHB_A$ AAA or BIM $SAHB_A$) technical replicates of islet cultures from one donor. **d**, Specific target engagement by BAD $SAHB_A$ SD as assessed by the capture of GK with biotinylated BAD $SAHB_A$ SD but not BAD $SAHB_A$ AAA or BIM $SAHB_A$ in INS-1 protein lysates. Western blot with the anti-PC antibody serves as negative control for GK. Input denotes INS-1 lysates not incubated with any stapled peptides or vehicle. Representative experiment is shown out of n = 2 experiments with similar results. **e**, Isothermal titration calorimetry (ITC) measurements showing the binding of recombinant human GK to BAD $SAHB_A$ SD in a 1:1 stoichiometry with binding affinity (dissociation constant, *Kd*) of ~580 nM (left). ITC using the corresponding unstapled peptide is shown for comparison with a log higher *Kd* (right). Data are representative of n = 3 independent ITC experiments with similar results. **f**, Western blots showing efficiency of *GK* knockdown in islets used in Figs. 1d and 2d. Blots are representative of n = 2 independent experiments with similar results.

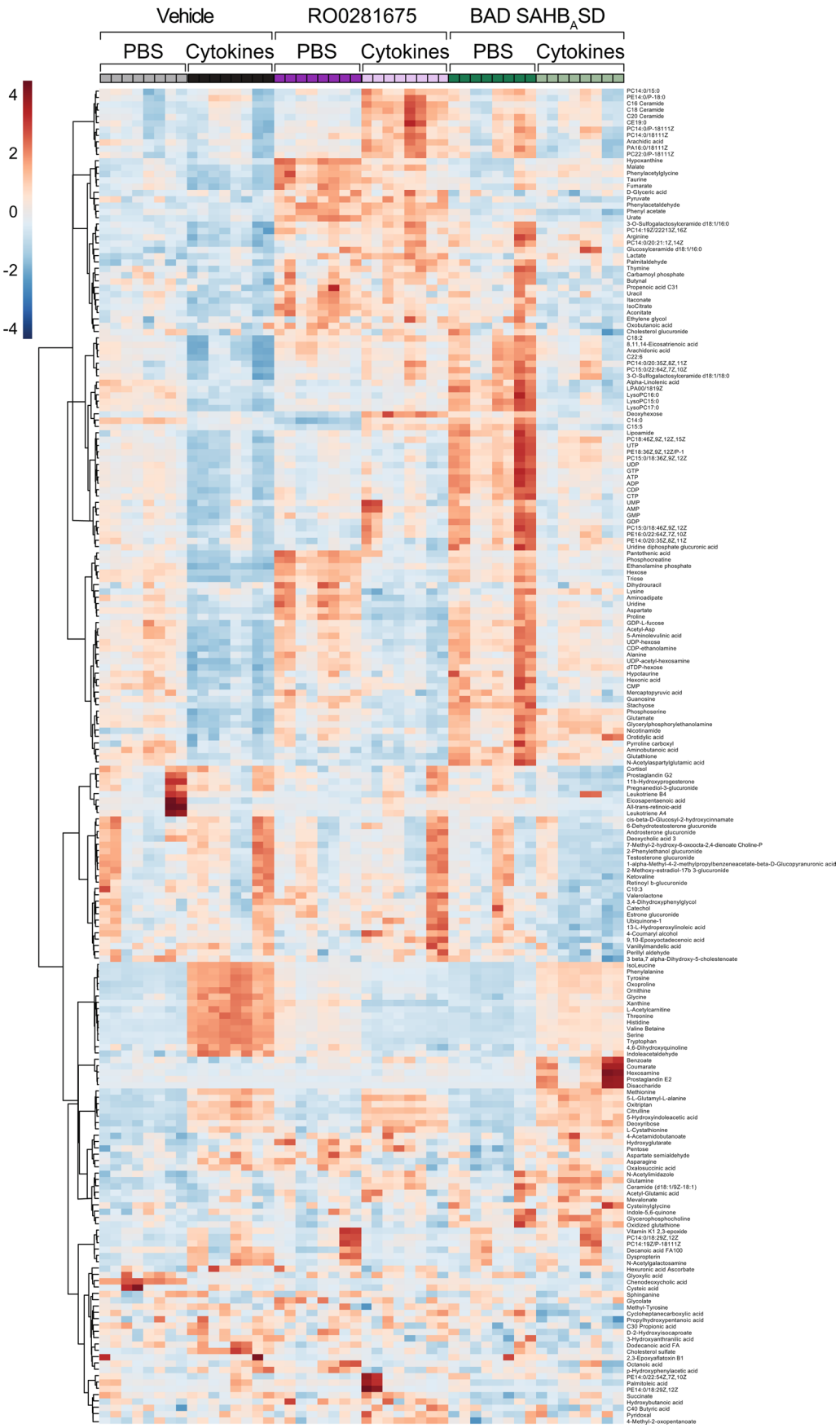

Extended Data Fig. 2 | Untargeted metabolomics analysis of human islets undergoing inflammation stress. Heatmap presentation of LC-MS untargeted metabolomics analysis of human islets showing PBS and cytokine conditions corresponding to Fig. 1h, i. Data are transformed into log fold change for heatmap presentation with 8 technical replicates of total ion counts shown for islets pooled from n = 5 human donors.

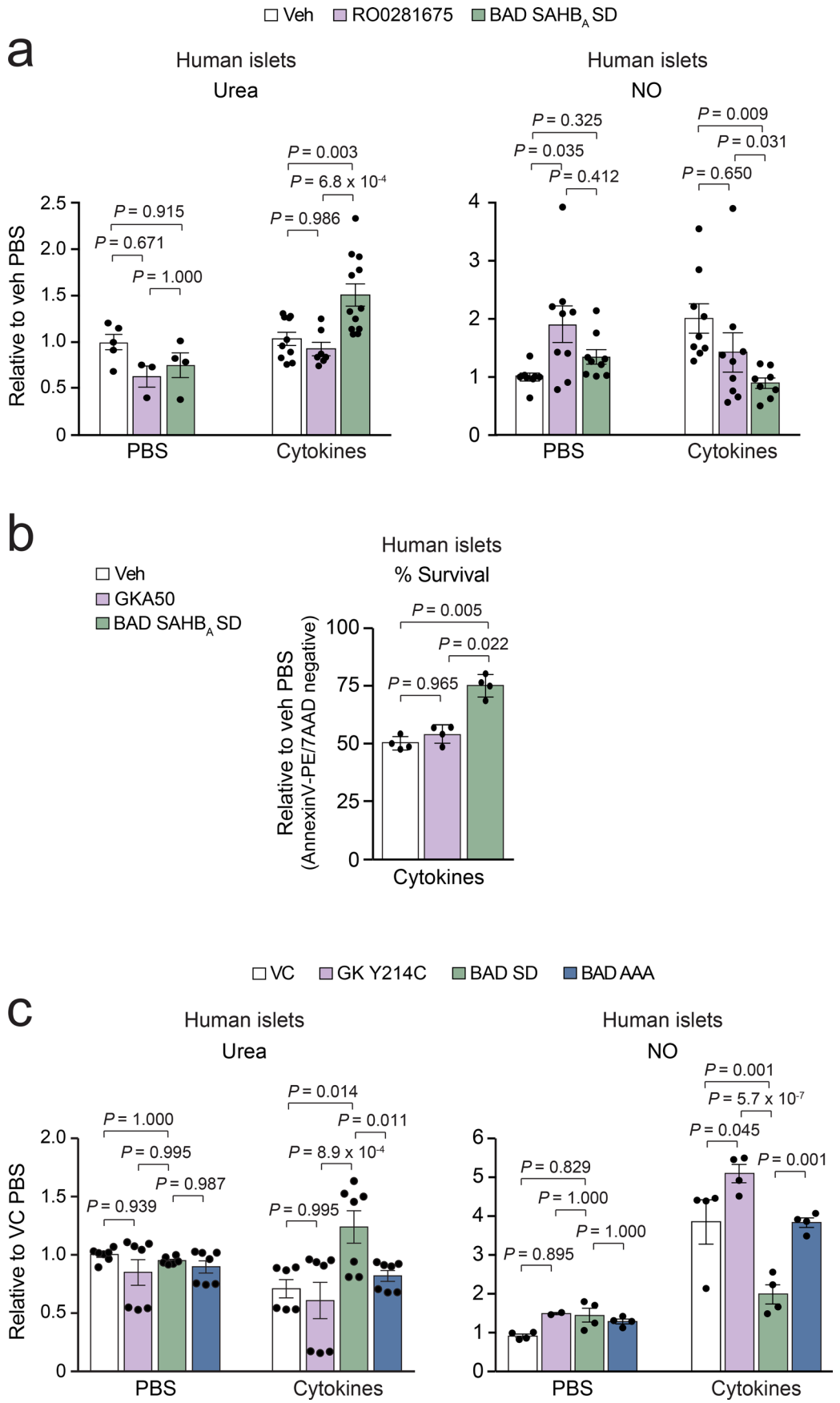

Extended Data Fig. 3 | See next page for caption.

Extended Data Fig. 3 | Altered arginine metabolism in the context of protective vs non-protective glucose metabolism. a, Urea and NO levels in human islets treated with the indicated compounds and exposed to cytokines (Fig. 2b), expanded to show the PBS data. PBS urea data are from n = 5 (Veh), n = 3 (RO0281675) and n = 4 (BAD $SAHB_A$ SD) human donors. Cytokine urea data are from n = 10 (Veh), n = 7 (RO0281675), and n = 12 (BAD $SAHB_A$ SD) donors. PBS NO data are from n = 8 (Veh, RO0281675), and n = 9 (BAD $SAHB_A$ SD) donors. Cytokine NO data are from n = 9 (Veh, RO0281675) and n = 8 (BAD $SAHB_A$ SD) donors. **b**, Viability of human islets treated with vehicle (DMSO), the allosteric GK activator (GKA50) or BAD $SAHB_A$ SD and exposed to inflammatory cytokines as in Fig. 2c, n = 4 donors. **c**, Urea and NO levels in human islets expressing the indicated GK and BAD mutants and treated with cytokines (Fig. 2f), expanded to show the PBS data. Urea data for PBS and cytokine conditions are from n = 6 (VC) and n = 7 (GK Y214C, BAD SD and BAD AAA) independent experiments using islet cultures from 2 donors. PBS NO data are from n = 4 (VC), n = 2 (GK Y214C) and n = 4 (BAD SD and BAD AAA) independent experiments using islet cultures from 2 donors. Cytokine NO data are from n = 4 (VC, GK Y214C, BAD SD and BAD AAA) independent experiments using islet cultures from 2 donors. Statistical analyses in (**a**) and (**c**) are two-way ANOVA and one-way ANOVA in (**b**), both with Tukey adjustment for multiple comparisons.

RNAseq analysis of urea cycle enzymes and related pathways in sorted β-cells and negative-sorted islet cells relative to whole islets

Gene name	β-cell	Whole islet	Non-β-cell
Urea cycle and related pathways			
ARG2	6.39	1	0.87
ASL	6.10	1	0.61
ASS1	5.05	1	1.03
CPS1	1.72	1	0.45
GOT1	5.09	1	1.29
GOT2	2.68	1	0.81
MDH1	10.09	1	1.02
MDH2	6.74	1	0.90
NAGS	3.16	1	1.60
OAT	10.22	1	1.64
PC	4.87	1	0.88
SLC25A12	9.97	1	1.46
SLC25A13	7.10	1	0.99
SLC25A15	1.90	1	0.68
Hormones			
INS	1.48	1	0.09
GCG	0.17	1	4.46
β-cell genes			
GCK	1.60	1	1.00
SLC2A2	3.47	1	0.28
MAFA	2.65	1	0.21
α-cell and non-β-cell genes			
ARX	0.13	1	1.86
DNMT1	0.76	1	0.93
LDHA	0.45	1	0.60

Extended Data Fig. 4 | Expression of urea cycle enzymes and related pathways in FACS-purified human β-cells subjected to transcriptomic analyses. RNAseq analysis of urea cycle enzymes and related pathways in sorted human β-cells and negative-sorted islet cells relative to whole islets. Read counts as RPKM (reads per kilobase per million mapped reads) are normalized to whole islet PKRM to assess enrichment. All urea cycle related enzymes and transporters are enriched (>1) in the β-cell fraction compared to whole islets and the negative-sorted cells.

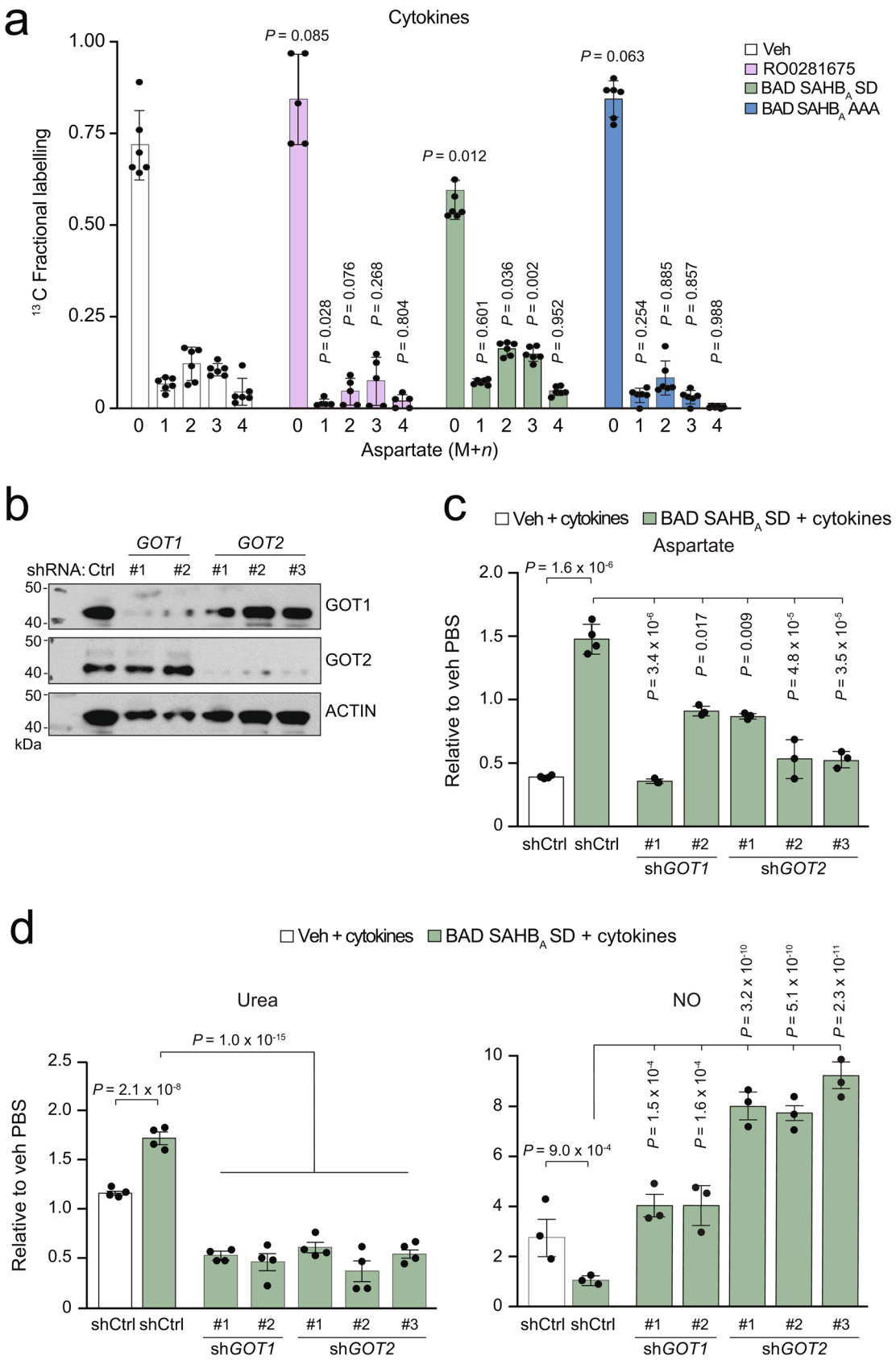

Fu et al. Extended Data Fig. 5

Extended Data Fig. 5 | See next page for caption.

Extended Data Fig. 5 | Increased generation of aspartate from glucose following protective GK activation. a, ^{13}C fractional labelling of aspartate from $^{13}C_6$ glucose. Data are shown as non-normalized to vehicle PBS and display the fraction of each M+*n* mass isotopomer out of the total pool of aspartate for each condition. For clarity, statistical comparisons are only shown for each M+*n* of a given condition (RO0281675, BAD $SAHB_A$ SD and BAD $SAHB_A$ AAA) compared to the corresponding M+*n* of vehicle control. Data are pooled means from n = 6 (Veh), n = 5 (RO0281675), and n = 6 (BAD $SAHB_A$ SD, BAD $SAHB_A$ AAA) independent mouse islet isolations and experiments. **b**, Western blot analysis of *GOT1/2* knockdown efficiency using multiple independent hairpins for data shown in Fig. 4d, e and Extended Data Fig. 5c,d. Blots are representative of n = 2 independent experiments with similar results. **c, d**, Aspartate (**c**), urea and NO (**d**) levels in human islets from the same experiments shown in Fig. 4d,e, displaying the complete set of data on all hairpins tested. Aspartate data are from n = 4 human donors for shCtrl samples and n = 3 donors for knockdown samples. Urea and NO data are from n = 4 and n = 3 donors, respectively. Statistical analyses in (**a**) are two-way ANOVA showing p-value comparisons for each condition to Veh, and one-way ANOVA in (**c**-**d**), both with Tukey adjustment for multiple comparisons.

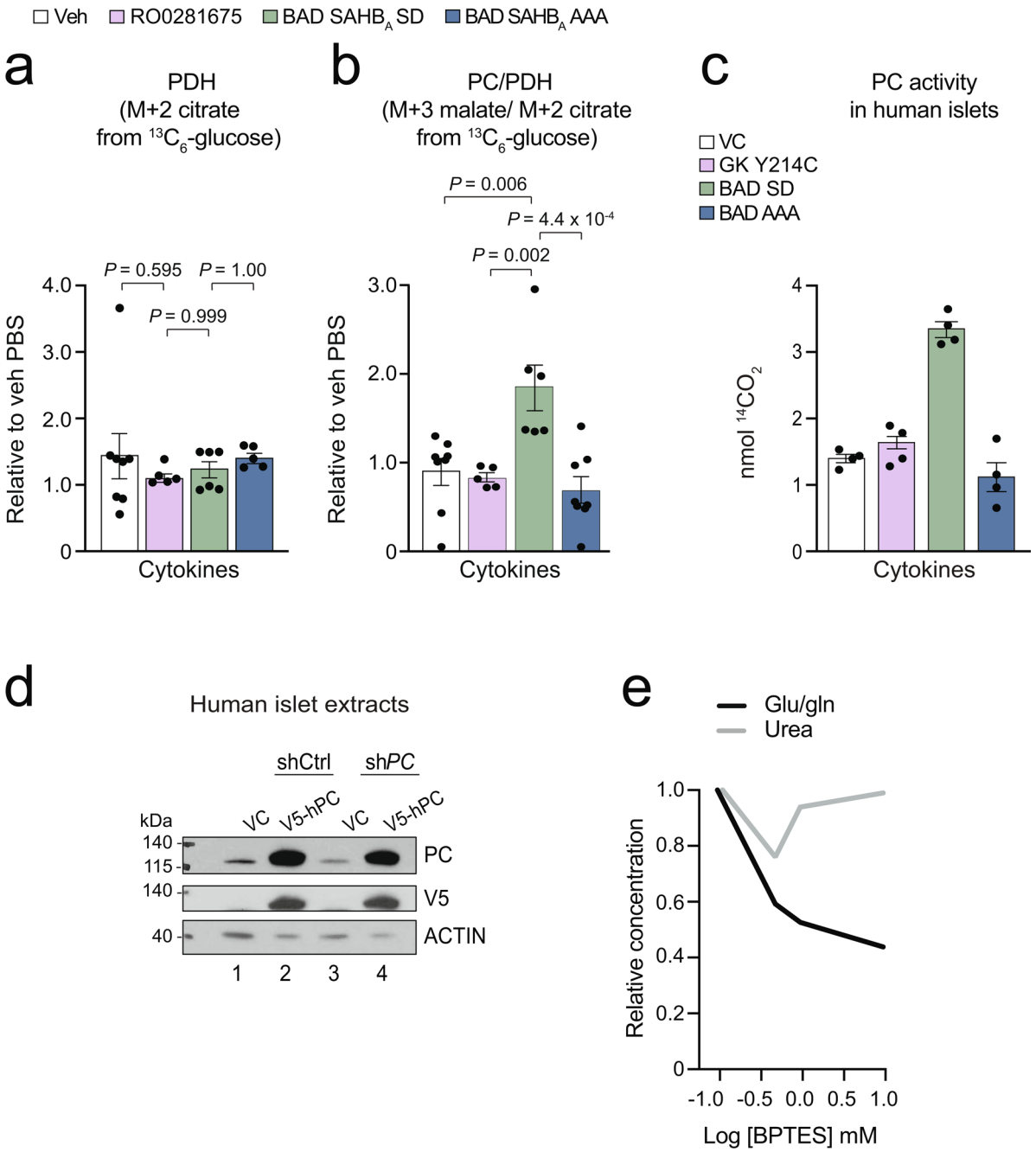

Extended Data Fig. 6 | Protective glucose metabolism increases pyruvate carboxylase activity in islets undergoing inflammation stress. a, b, PDH (**a**) and the ratio of PC/PDH (**b**) activity in mouse islets labeled with $^{13}C_6$ glucose, measured as M+2 citrate and the ratio of M+3 malate to M+2 citrate, respectively. Data are from analogous glucose tracer studies as in Fig. 5a, showing n = 8 (Veh), n = 5 (RO0281675, BAD SAHB$_A$ AAA) and n = 6 (BAD SAHB$_A$ SD) independent experiments for PDH, and n = 8 (Veh, BAD SAHB$_A$ AAA), n = 5 (RO0281675) and n = 6 (BAD SAHB$_A$ SD) independent experiments for PC/PDH. Statistical analyses were performed using one-way ANOVA with Tukey adjustment for multiple comparisons. **c**, PC activity in human islets treated with inflammatory cytokines in the context of protective vs non-protective glucose metabolism. Enzyme activity was measured as nmol $^{14}CO_2$ generated from $NaH^{14}CO_3$, n = 2 human donors in duplicate. **d**, Validation of on-target *PC* knockdown and expression level of V5-tagged human PC (hPC) cDNA used to rescue PC expression in human islets treated with a 3′UTR-targeted shRNA against *PC* in experiments corresponding to Fig. 5d. Blots are representative of n = 2 independent experiments with similar results. **e**, The GLS inhibitor BPTES (Bis-2-(5-phenylacetamido-1,3,4-thiadiazol-2-yl)ethyl sulfide) does not affect islet urea levels at concentrations that reduce the ratio of glutamate/glutamine (glu/gln, a readout of GLS activity), n = 2 human donors.

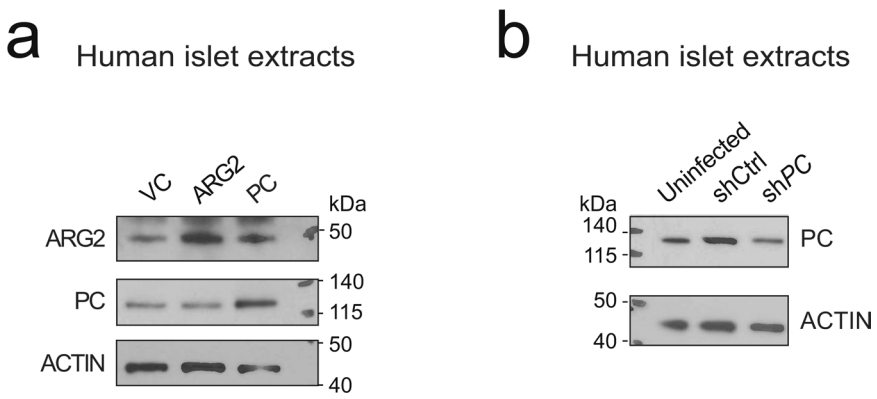

Extended Data Fig. 7 | Validation of ARG2 and PC overexpression and knockdown. a, Western blot analysis of ARG2 and PC expression levels in human islets corresponding to experiments shown in Fig. 7a,b,h,i. Blots are representative of n = 2 independent experiments with similar results. **b**, Western blot analysis of *PC* knockdown efficiency in experiments corresponding to Fig. 7c–e. Blots are representative of n = 3 independent experiments with similar results.

nature research

Corresponding author(s): Nika N Danial

Last updated by author(s): 16/03/20

Reporting Summary

Nature Research wishes to improve the reproducibility of the work that we publish. This form provides structure for consistency and transparency in reporting. For further information on Nature Research policies, see Authors & Referees and the Editorial Policy Checklist.

Statistics

For all statistical analyses, confirm that the following items are present in the figure legend, table legend, main text, or Methods section.

n/a	Confirmed
☐	☒ The exact sample size (*n*) for each experimental group/condition, given as a discrete number and unit of measurement
☐	☒ A statement on whether measurements were taken from distinct samples or whether the same sample was measured repeatedly
☐	☒ The statistical test(s) used AND whether they are one- or two-sided *Only common tests should be described solely by name; describe more complex techniques in the Methods section.*
☐	☒ A description of all covariates tested
☐	☒ A description of any assumptions or corrections, such as tests of normality and adjustment for multiple comparisons
☐	☒ A full description of the statistical parameters including central tendency (e.g. means) or other basic estimates (e.g. regression coefficient) AND variation (e.g. standard deviation) or associated estimates of uncertainty (e.g. confidence intervals)
☐	☒ For null hypothesis testing, the test statistic (e.g. *F*, *t*, *r*) with confidence intervals, effect sizes, degrees of freedom and *P* value noted *Give P values as exact values whenever suitable.*
☒	☐ For Bayesian analysis, information on the choice of priors and Markov chain Monte Carlo settings
☐	☒ For hierarchical and complex designs, identification of the appropriate level for tests and full reporting of outcomes
☒	☐ Estimates of effect sizes (e.g. Cohen's *d*, Pearson's *r*), indicating how they were calculated

Our web collection on statistics for biologists contains articles on many of the points above.

Software and code

Policy information about availability of computer code

Data collection	GraphPAD Prism 8, Microsoft Excel 2020, BD FACSDIVA software 8, Agilent MassHunter Qualitative Analysis 4.2, Agilent MassHunter Quantitative Analysis 4.2, Tracefinder 3.3, Metamorph 10, Bioanalyzer, Qubit and Metaboanalyst 4.0.
Data analysis	GraphPAD Prism 8, Microsoft Excel 2020, BD FACSDIVA software 8, Agilent MassHunter Qualitative Analysis 4.2, Agilent MassHunter Quantitative Analysis 4.2, Tracefinder 3.3, Metaboanalyst 4.0, PEAK studio 10.0., Pep2gene tool v1, NanoAnalyze software v1, Fiji V2.0.

For manuscripts utilizing custom algorithms or software that are central to the research but not yet described in published literature, software must be made available to editors/reviewers. We strongly encourage code deposition in a community repository (e.g. GitHub). See the Nature Research guidelines for submitting code & software for further information.

Data

Policy information about availability of data

All manuscripts must include a data availability statement. This statement should provide the following information, where applicable:

- Accession codes, unique identifiers, or web links for publicly available datasets
- A list of figures that have associated raw data
- A description of any restrictions on data availability

The complete beta cell proteomic dataset with accession codes is available publicly at https://www.ebi.ac.uk/pride/archive/.

Field-specific reporting

Please select the one below that is the best fit for your research. If you are not sure, read the appropriate sections before making your selection.

☒ Life sciences ☐ Behavioural & social sciences ☐ Ecological, evolutionary & environmental sciences

For a reference copy of the document with all sections, see nature.com/documents/nr-reporting-summary-flat.pdf

Life sciences study design

All studies must disclose on these points even when the disclosure is negative.

Sample size	When possible at least n=5 donors was used to verify treatment-dependent effects. Due to limited donor availability the following studies had the following sample sizes: GK knockdown; n=2-4 donors, NPG for beta-cell and viability costaining; n=1 donor with 4 replicates, INS1 cell studies n=4 technical replicates, Full-length BAD and GK mutant expression studies; n=2 donors, GK actvity; n=1 donor in 3 replicates, ITC data was n=3 experimental repeats, GKA50 studies; n=2-4 donors, RNAseq studies; n=3 donors, proteomic analysis; n=3 donors, PC activity; n=2 donors, GLS inhibitor BPTES studies; n=2 donors, arginine and PC overexpression rescue n=3-4 donors due to limited tissue availability. In the case of the Type 2 diabetic islets n=2 donors in triplicate cultures. For in vivo transplant studies, n=7-12 mice per condition in total were endpointed separately in that n=4-6 mice were enpointed at Day 2 post-transplantation for TUNEL staining to quantify human beta cell death measurements within the grafts, while n=3-6 mice were monitored for blood glucose and insulin levels up to the Day 49 post transplant endpoint.
Data exclusions	All data were included for all analyses. In few and limited cases outlier removal criteria were pre-determined by using GraphPad statistical analysis software 8, first identified with two-sided Grubbs with alpha = 0.05, in the case that an outlier was observed then the data were further inspected with the ROUT method at FDR set to 1% to check for multiple outliers. The following experiments had one or two outliers removed for one condition: beta cell death measurements in grafts, aspartate 13C data for the glucose tracer, and urea M+2 from the arginine tracer, and NO levels from one human donor were left out which had a response to treatment more than 2 s.d.'s outside the entire set of means.
Replication	Replication of experimental findings were performed on different days with different donors each time. Treatments had reproducible effects except when viability of the donor material was below 50% for control at baseline/untreated. In all but 3 experiments mouse islet or INS1 cell results were recapitulated in human donor material, selected based on several criteria: priority of finding, requirement of material for robust data collection, and donor availability.
Randomization	The entire pool of islets for a given donor was always used across all conditions in a given experiment for internal within-donor comparison, and donors were randomly used for a given type of experiment based on availability and depending on the direction in which the study was going at the time of receiving a given donor. Isolated mouse islets were always pooled from different wild type mice and used across all conditions without bias.
Blinding	Blind analysis was performed during the TUNEL staining in the islets graft, where stained sections of grafts were coded by number. Almost all cases of sample preparation for biochemical and GCMS analyses were performed blind as samples were numbered and conditions were identified after the experiments were performed. All LCMS samples were analyzed outside of the corresponding authors lab and samples were run blind by the facilities operators. Proteomic studies and RNAseq analyses here were non-biased data acquisition platforms that did not require blinding as they were strictly descriptive.

Reporting for specific materials, systems and methods

We require information from authors about some types of materials, experimental systems and methods used in many studies. Here, indicate whether each material, system or method listed is relevant to your study. If you are not sure if a list item applies to your research, read the appropriate section before selecting a response.

Materials & experimental systems

n/a	Involved in the study
☐	☒ Antibodies
☐	☒ Eukaryotic cell lines
☒	☐ Palaeontology
☐	☒ Animals and other organisms
☒	☐ Human research participants
☒	☐ Clinical data

Methods

n/a	Involved in the study
☒	☐ ChIP-seq
☐	☒ Flow cytometry
☒	☐ MRI-based neuroimaging

Antibodies

Antibodies used	For western blot analysis: -BCl2-associated death promoter antibody from Abcam rabbit monoclonal antibody ab32445, cloneY208, lot#GR149036-1, validated for WB in human and mouse used at 1:3000.

-Glucokinase rabbit polyclonal antibody from Santa Cruz, sc-7908 Lot# G2815 clone H88, validate for western blot in human and mouse used at 1:1000.
-GOT1/AST1 antibody from Sino Biological, cat#14196-T52, H07E; P17174; Met1-Gln413, validated for western blot in humna, used at 1:1000.
-GOT2/AST2 rabbit polyclonal antibody from MyBioSource MBS2003146, validated for western blotting in human, used at 1:1000.
-pyruvate carobxylase was detected with mouse monoclonal Santa Cruz anitbody PCB clone H-2, CAT#sc-271493, lot# C1413 validated for WB in human and mouse used at 1:1000.
-arginase2 was detected with a polyclonal rabbit antibody from Life technologies, Cat# PA5-27987, Lot# SC2363791C validated for WB in human and mouse used at 1:1000.
-V5 tag detected with rabbit monoclonal antibody against V5 from Cell Signaling clone D3H8Q, Cat#13202S, Lot:2 validated for WB used at 1:1000.
-MYC-tag 9B11 mouse monoclonal antibody from Cell Signaling, Cat##2276, validated for WB of MYC tags, used at 1:1000.
-actin was detected with a mouse monoclonal antibody from Sigma clone AC-15, Cat#A5441, validated for WB in human and mouse used at 1:20,000.
For immunofluorescence:
- a polyclonal anitbody against insulin was used at 1:100 from DAKO #A0564, produced in pig based on protein P01315 and validated for immunohistochemistry and immunofluorescence.
-arginase2 was detected with a polyclonal rabbit antibody from ABClonal, Cat# A6355, validated for use in western blotting.
-argininosuccinate lyase was detected with a rabbit polyclonal antibody from Millipore Sigma, Cat#AV41666, validated for use in western blot.
-argininosuccinate synthase was detected with a mouse monoclonal antibody from Thermo Fisher Scientific, Cat#MA5-17033, validated for use in immunofluorescence.
-carbamoyl synthase 1 was detected with an a polyclonal rabbit antibody from ABClonal, Cat#A8080, validated for use in immunofluorescence.
-N-acteylglutamate synthase was detected with an a polyclonal rabbit antibody from ABClonal, Cat#A12086, validated for use in western blotting.
-Dimethylarginine dimethylaminohydrolase 1 was detected with a rabbit polyclonal antibody from Sino Biologicals, Cat#102610-T10, validated for immunofluorescence.
-Dimethylarginine dimethylaminohydrolase 2 was detected with a rabbit polyclonal antibody from ABCLonal, Cat#A6457, validated for immunofluorescence.

Validation

For western blot analysis:
-BCl2-associated death promoter -Abcam rabbit monoclonal antibody ab32445, cloneY208, lot#GR149036-1, validated for WB in human and mouse
Glucokinase rabbit polyclonal antibody from Santa Cruz, sc-7908 Lot# G2815 clone H88, validate for western blot in human and mouse used at 1:1000.
-GOT1/AST1 antibody from Sino Biological, cat#14196-T52, H07E; P17174; Met1-Gln413, validated for western blot in humna, used at 1:1000.
-GOT2/AST2 rabbit polyclonal antibody from MyBioSource MBS2003146, validated for western blotting in human, used at 1:1000.
-pyruvate carobxylase -mouse monoclonal Santa Cruz anitbody PCB clone H-2, CAT#sc-271493, lot# C1413 validated for WB in human and mouse used at 1:1000.
-arginase2 -polyclonal rabbit antibody from Life technologies, Cat# PA5-27987, Lot# SC2363791C validated for WB in human and mouse used at 1:1000.
-V5 tag - rabbit monoclonal antibody from Cell Signaling clone D3H8Q, Cat#13202S, Lot:2 validated for WB used at 1:1000.
-MYC-tag 9B11 mouse monoclonal antibody from Cell Signaling, Cat##2276, validated for WB of MYC tags, used at 1:1000.
-actin -mouse monoclonal antibody from Sigma clone AC-15, Cat#A5441, validated for WB in human and mouse used at 1:20,000.

For immunofluorescence:
- a polyclonal anitbody against insulin was used at 1:100 from DAKO #A0564, produced in pig based on protein P01315 and validated for immunohistochemistry and immunofluorescence.
-arginase2 was detected with a polyclonal rabbit antibody from ABClonal, Cat# A6355, validated for use in western blotting.
-argininosuccinate lyase was detected with a rabbit polyclonal antibody from Millipore Sigma, Cat#AV41666, validated for use in western blot.
-argininosuccinate synthase was detected with a mouse monoclonal antibody from Thermo Fisher Scientific, Cat#MA5-17033, validated for use in immunofluorescence.
-carbamoyl synthase 1 was detected with an a polyclonal rabbit antibody from ABClonal, Cat#A8080, validated for use in immunofluorescence.
-N-acteylglutamate synthase was detected with an a polyclonal rabbit antibody from ABClonal, Cat#A12086, validated for use in western blotting.
-Dimethylarginine dimethylaminohydrolase 1 was detected with a rabbit polyclonal antibody from Sino Biologicals, Cat#102610-T10, validated for immunofluorescence.
-Dimethylarginine dimethylaminohydrolase 2 was detected with a rabbit polyclonal antibody from ABCLonal, Cat#A6457, validated for immunofluorescence.

Eukaryotic cell lines

Policy information about cell lines

Cell line source(s)

INS1 cell lines were obtained from Don Scott and Richard Kibbey. For lentiviral production HEK293T cell line was obtained from Thermo Scientific Cat#HCL4517 .

Authentication	None of the cell lines used have been authenticated.
Mycoplasma contamination	Cell lines were tested for mycoplasma contamination by Thermo Scientific before purchase.
Commonly misidentified lines (See ICLAC register)	No commonly misidentified cell lines were used.

Animals and other organisms

Policy information about studies involving animals; ARRIVE guidelines recommended for reporting animal research

Laboratory animals	Wild type mice were bred from orignal C57/BL6 mice obtained from Jackson Laboratories. Male and female mice were included at random with ages 10-12 weeks old. A total of 22 NOD/Scid male mice were obtained from Jackson lab of the specific strain NOD.CB17-Prkdcscid/J and were used at 10-12 weeks.
Wild animals	This study did not involve wild animals.
Field-collected samples	This study did not include samples collected in the field.
Ethics oversight	All animal studies were performed in compliance with, and with approval of, the Icahn School of Medicine at Mount Sinai Institutional Animal Care and Use Committee. Islets were isolated from WT/c57BL6 mice with the approval of the Institutional Animal Care and Use Committee of Dana-Farber Cancer Instiute, protocol #097-2016.

Note that full information on the approval of the study protocol must also be provided in the manuscript.

Flow Cytometry

Plots

Confirm that:

☒ The axis labels state the marker and fluorochrome used (e.g. CD4-FITC).

☒ The axis scales are clearly visible. Include numbers along axes only for bottom left plot of group (a 'group' is an analysis of identical markers).

☐ All plots are contour plots with outliers or pseudocolor plots.

☐ A numerical value for number of cells or percentage (with statistics) is provided.

Methodology

Sample preparation	Samples were prepared from isolated human and mouse islets and were single-celled by gentle accutase dissociation. Cells were stained with AnnexinV/7aad (BD biosciences) for cell viability or DAF-FM (Invitrogen) for NO levels diacetate.
Instrument	BD FACS Canto II analyzer
Software	BD FACS Diva
Cell population abundance	For all experiments at least 10,000 cells were analyzed per sample.
Gating strategy	FSC (180V; 1QA 3-10A S), and SSC (150 V; 1QA 3-10A 4) gates were made on a homogenous cell populations. Unstained cells of the same preparation were used to define a cut-off threshold for classifying positive staining using the dyes for viability and NO levels, and for sorting uninfected cells from the same donor were used as FITC-negative threshold, in general this was above 1Q^3 signal intensity.

☒ Tick this box to confirm that a figure exemplifying the gating strategy is provided in the Supplementary Information.